Exhumation of basement-cored uplifts: Example of the Kyrgyz Range quantified with apatite fission-track thermochronology

Edward R. Sobel [1], Michael Oskin [2], Douglas Burbank [3], Alexander Mikolaichuk [4]

1 Institut fuer Geowissenschaften, Universitaet Potsdam, Postfach 601553, 14415 Potsdam, Germany, sobel@rz.uni-potsdam.de

2 Dept. of Geological Sciences, University of North Carolina at Chapel Hill, Chapel Hill, NC, USA 27599

3 Dept. of Geological Sciences, University of California, Santa Barbara, CA USA 93106

4 Institute of Geology, 30 Erkindyk Ave., Bishkek 720481, Kyrgyzstan

Abstract

The Kyrgyz Range, the northernmost portion of the Kyrgyzstan Tien Shan, displays topographic evidence for lateral propagation of surface uplift and exhumation. The highest and most deeply dissected segment lies in the center of the range. To the east, topography and relief decrease, and preserved remnants of a Cretaceous regional erosion surface imply minimal amounts of bedrock exhumation. The timing of exhumation of range segments defines the lateral propogation rate of the range-bounding reverse fault and quantifies the time and erosion depth needed to transform a mountain range from a juvenile to a mature morphology. New apatite fission-track (AFT) data from three transects from the eastern Kyrgyz Range, combined with published AFT data, demonstrate that the range has propagated over 110 km eastwards over the last 7-11 Myr. Based on the thermal and topographic evolutionary history, we present a model for a time-varying exhumation rate driven by rock uplift and changes in erodability and the time scale of geomorphic adjustment to surface uplift. Easily eroded, Cenozoic sedimentary rocks overlying resistant basement control early, rapid exhumation and slow surface uplift rates. As increasing amounts of resistant basement are exposed, exhumation rates decrease while surface uplift rates are sustained or increase, thereby growing topography. As the range becomes high enough to cause ice accumulation and develop steep river valleys, fluvial and glacial erosion become more powerful and exhumation rates once again increase. Independently determined range-normal shortening rates have also varied over time, suggesting a feedback between erosional efficiency and shortening rate.

Introduction

Growth of a contractional mountain range is driven by an evolving relationship between rock uplift, surface uplift, and exhumation. Surface uplift is defined as rock uplift minus exhumation [*England and Molnar*, 1990]. In the early phase of orogenesis, rock uplift must outpace exhumation; in a steady-state orogen, these reach an equilibrium, while in the final, destructive

phase of an orogen, exhumation dominates [e.g., *Willett and Brandon*, 2002]. Temporal changes in key controlling factors, such as fault geometry, shortening rate, and erosion rate will influence the surface uplift history [e.g., *Burbank et al.*, 1996; *Abbott et al.*, 1997; *Stock and Montgomery*, 1999; *Whipple and Tucker*, 1999]. Erosion rate may be controlled by factors such as channel gradients, surface slopes, relief, precipitation, glacial extent, and rock resistance [e.g., *Ahnert*, 1970; *Howard*, 1994; *Brozovic et al.*. 1997; *Hallet et al.* 1996; *Schmidt and Montgomery*, 1996; *Sklar and Dietrich*, 2001; *Whipple*, 2004]. Perhaps because complex interactions among these factors undoubtedly occur, the detailed evolution and interdependence of these factors is rarely delineated.

Reverse-fault-bounded mountain ranges propagating into a foreland basin commonly initiate either as a single, localized structure which gradually lengthens along strike with increasing amount of shortening, or as several fault segments which eventually coalesce or overlap [*Dawers*, 1993; *Cartwright et al.*, 1995]. In either case, the active range-front likely lengthens as displacement accumulates on the range-bounding faults. After several million years of displacement, the original, relatively small structures may be impossible to discern. However, if a reference horizon along the trend of the range exists, range growth and exhumation can be placed into a topographic reference frame by combining low-temperature thermochronologic data with structural geology and geomorphic analysis. When ranges grow through lateral and vertical propagation, a space-for-time substitution can illuminate the long-term spatial and temporal distribution of exhumation and surface uplift and can permit reconstruction of progressive changes in the balance between rock uplift and exhumation [*Burbank et al.*, 1999]. Space-for-time substitutions are most reliable when time constraints exist for the interval of range propagation. Such along-strike temporal control, however, is commonly lacking in most studies of fold-and-thrust belts. Only when reliable ages can be assigned to various stages of range growth can the validity of the substitution be assessed. We report here a time-calibrated example of range propagation from the Kyrgyz Tien Shan.

The Kyrgyz range of the northern Tien Shan (Figure 1) provides an example of a reverse-fault bounded mountain range with topographic evidence for progressive lateral propagation of surface uplift and exhumation. The highest and most deeply dissected sector of the range lies in its central portion, south of Bishkek, in the region of the Ala Archa River. Glaciers mantling peaks up to 4800 m have deeply dissected the granitic range in this region, and reset apatite fission-track and U-Th/He thermochronometers indicate >5 km of exhumation at river level [*Bullen et al.*, 2003]. To the east and west, both topography and relief decrease. Moreover, preservation of remnants of a Cretaceous regional erosion surface [*Trofimov et al.*, 1976] implies minimal amounts of bedrock exhumation. If the timing of exhumation of segments of the range outward from the center can be defined, the lateral propagation rate of the range can be estimated and the depth of erosion and time needed to transform a mountain range from a juvenile to a mature morphology can be reconstructed.

Here we present new apatite fission-track (AFT) data from three transects from the eastern half of the Kyrgyz Range that, when combined with published AFT data, demonstrate that the range has propagated over 110 km from the presently highest region towards the east over the last 7-11 Myr. When synthesized with structural data and analysis of recently produced digital topography, we can reconstruct the thermal and topographic evolutionary history of the Kyrgyz range. We present a model for a time-varying exhumation rate driven by the interplay of rock erodability, surface processes, and shortening rate. We propose that easily eroded Cenozoic sedimentary rocks that overlie resistant pre-Tertiary bedrock control early, rapid exhumation and slow surface uplift rates. As increasing amounts of resistant bedrock are exposed, exhumation and shortening rates decrease while surface uplift can persist, thereby growing topography. This decrease in shortening rate may be counterbalanced by basinward-propagation of the deformation front. As the range becomes high enough to cause ice accumulation and orographically enhanced precipitation, fluvial and glacial erosion become more effective and exhumation rates once again increase. A balance between

erosion and rock uplift occurs through establishment of mature drainage networks into the range that connect high-elevation glaciated areas to deeply incised rivers. Based on analysis of the digital topography, we argue that the central part of the range has achieved this balance and represents a topographic steady state.

Geologic history

The Tien Shan records a complex Paleozoic history of island arc accretion [*Burtman* 1975; *Carroll et al.*, 2001; *Bazhenov et al.*, 2003] followed by Permian strike-slip deformation [*Burtman* 1975; *Bazhenov et al.*, 1999]. Episodes of intracontinental deformation driven by distal plate margin tectonism occurred during the Early-Middle Jurassic and the Late Jurassic-Cretaceous, documented by foreland-basin formation to the north and south of the Tien Shan, as well as in a prominent transtensional basin cross-cutting the range [*Hendrix et al.*, 1992; *Sobel*, 1999]. Apatite fission-track data suggest pulses of exhumation during the Permian and the Jurassic [*Sobel and Dumitru*, 1997; *Bullen et al.*, 2001; *Dumitru et al.*, 2001]; these are likely correlated with episodes of deformation within the Tien Shan and deposition within the Tarim basin.

A widespread regional erosion surface formed within the central Kyrgyz Tien Shan in the late Mesozoic [*Trofimov et al.*, 1976; *Makarov*, 1977; *Chediya*, 1986; see *Burbank et al.*, 1999 for photographs]. This surface is unconformably overlain by the Paleocene-Eocene Suluterek formation (also called the Kokturpak formation), containing calcareous sandstone, dolomite, gypsum, and an arid spore-pollen assemblage [*Chediya et al.*, 1973; *Fortuna et al.*, 1994] as well as localized Eocene basalt flows [*Krylov*, 1960]. The formation is typically ca 150 m thick and is truncated by an erosional unconformity separating it from upper Tertiary sediments [*Chediya et al.*, 1973; *Fortuna et al.*, 1994]; drilling in the Chu basin reveals that the thickness locally reaches 635 m [*Burg et al.*, 2004]. Overall, this Mesozoic to Tertiary interval of erosion and minor deposition

spans ca. 100 Myr period of tectonic quiescence, during which a stable thermal regime in the upper crust was established [*Bullen et al.*, 2001].

The Cenozoic exhumation history of the Tien Shan has been used to study the evolution of the range. Fission-track cooling ages and deposition of apparently syntectonic conglomerates in the adjacent Tarim basin suggest that shortening commenced around the Oligocene – Miocene boundary [*Hendrix et al.*, 1994; *Sobel and Dumitru*, 1997; *Yin et al.*, 1998]. This intracontinental deformation is driven by the Eocene – present collision of India with Asia. Deformation within the Tien Shan between 73-80°E longitude (Fig. 1) appears to have begun along the southern side of the range adjacent to the Tarim Basin at ca. 26 Ma and then propagated northwards across the individual ranges of the Tien Shan [*Sobel et al.*, 2000; *Dumitru et al.*, 2001]. Deformation has not propagated monotonically northward; at least the last several million years of this history have been marked by deformation throughout the entire range [*Thompson et al.*, 2002]. At present, seismicity is distributed throughout the width of the orogen [*Bune and Gorshkov*, 1980] and geodetic studies document a continuous gradient of shortening between Kashgar and Bishkek [*Abdrakhmatov et al.*, 1996; *Reigber et al.*, 2001]. Exhumation of the Kyrgyz range on the northern margin of the Tien Shan began in the region of Ala Archa (Fig. 2) at ~11 Ma [*Bullen et al.*, 2001]. Deformation is dominantly north-vergent thrusting, with a minor sinistral transpressional component [e.g., *Cobbold et al.*, 1996; *Mikolaichuk*, 2000; *Thompson et al.*, 2002] (Fig. 2).

The Oligocene-Miocene Shamsi Formation, exposed in the southern margin of the Chu Basin, was deposited in a foreland basin that pre-dated growth of the Kyrgyz Range [*Bullen et al.*, 2001]. The thickness of the pre-11 Ma sediment in the Chu basin is ca. 1 km. Although it is difficult to constrain the amount of Cenozoic sediment that formerly overlay the Kyrgyz range, it likely exceeded the amount in the Chu basin because of flexural subsidence of the Kyrgyz Range in advance of the northward propagating Tien Shan uplift. This pre-11 Ma burial contributed to the maximum temperature experienced by basement samples during the Neogene. During subsequent

exhumation, the weakly lithified Neogene sediment could be more readily eroded than the underlying Paleozoic strata. The Chu basin is deepest in the region of Bishkek and becomes shallower to the east, west, and north [*Abdrakhmatov et al.*, 2001] (Figure 2), suggesting that the magnitude of flexural subsidence and hence the amount of thrusting in the Kyrgyz range is greatest in the central section of the range. *Bullen et al.* [2001; 2003] present a detailed basin and tectonic analysis based on the stratigraphy and magnetostratigraphy of the last ca. 9 Ma of the Chu basin fill combined with structural and apatite U-Th/He and fission-track thermochronologic studies of the central Kyrgyz range. This work demonstrates that the range was rapidly exhumed between 11 and 10 Ma along a north-vergent thrust; deformation and cooling rates decreased significantly for the next 7 Myr until 3 Ma, when rates increased again. The deformation front propagated slightly between 8 and 3 Ma, coinciding with coarsening-upwards deposition in the basin. During the last 3 Myr, sediment accumulation rates reached a maximum, while the Kyrgyz range was being rapidly exhumed; deformation propagated farther into the foreland, forming a piggyback basin.

Geomorphology and Neotectonics

GPS measurements indicate ~20 mm/yr of modern shortening across the central Tien Shan: nearly half of the total convergence rate between India and Asia [*Abdrakmatov et al.*, 1996; *Reigber et al.*, 2001]. This shortening is distributed across a 400-km-wide belt of subparallel ranges and intramontane basins that are separated by active reverse faults [*Thompson et al.*, 2002]. The Kyrgyz Range forms the northernmost topographic crest within the central Tien Shan. Young thrust-fault scarps and seismicity along the northern margin of the range [*Chediya et al.*, 1998; *Thompson et al.*, 2002] attest to ongoing shortening. These ranges form an orographic barrier, with precipitation focused on the northern flanks [*Aizen et al.*, 1995].

From a structural perspective, a propagating range would be expected to exhibit increasing amounts of rock uplift and structural relief as a function of distance from the tip toward the center

of the range. From a geomorphological perspective, the temporal lag between surface uplift and erosional response [*Kooi and Beaumont*, 1996; *Willett*, 1999] suggests that relief, peak height, hillslope angles, and mean elevation should all initially increase as the range grows. As a range approaches or attains a topographic steady state, relief, mean elevation, and hillslope angles should stabilize. Hillslope angles, topographic relief, and hypsometry were derived from the 3-arcsec DEM (SRTM, 2003) resampled into Universal Transverse Mercator projection with 70 m pixels. Hillslope angle, mean and maximum elevation of the Kyrgyz Range all attain average values within 50 km of its eastern tip, supporting the contention that range-scale topographic steady state may prevail over the majority of the range (Fig. 1c).

A view of the early stages of geomorphic evolution of the Kyrgyz range is provided by observations of uplifted and deformed remnants of the pre-Cenozoic erosion surface on its southeastern slope (Fig. 3). This exhumed unconformity surface is recognized in the field and on remote sensing images as concordant, uniformly tilted regions etched by a distinctive dendritic network of shallow bedrock channels [*Oskin and Burbank, Alpine landscape evolution dominated by cirque retreat, submitted manuscript to Geology, hereafter referred to as Oskin and Burbank, submitted manuscript*]. On the southern flank of the Kyrgyz Range, southward tilting of the erosion surface remnants increases from east to west, consistent with a model of increasing displacement and range-scale limb rotation above a listric thrust fault [*Erslev*, 1986], such as is proposed to underlie the Kyrgyz Range [*Abdrakhmatov et al.*, 2001]. Field observations at the southern foot of the range and at other nearby outcrops of the erosion surface indicate that it is exhumed from beneath easily eroded Cenozoic continental sedimentary rocks. Remnants of the erosion surface can be traced from the foot of the range to the range crest in the easternmost south-facing slope of the Kyrgyz Range. Outcrops of the erosion surface diminish westward in response to progressively greater range uplift above the Pleistocene glacial equilibrium line altitude (ELA), and corresponding incision of glaciated valleys into bedrock. North-facing glaciated valleys also

expand laterally via cirque retreat into low-relief south-facing erosion surface remnants [*Oskin and Burbank*, submitted manuscript]. This process expands the area covered by north-flowing glaciers (Fig. 3) and moves the drainage divide relatively southward.

Morphometric analyses of drainage basins that descend from the crest of the Kyrgyz Range link catchment-scale erosion and relief generation to range-scale topographic development. Most of our morphometric analyses focused on the north-facing catchments that reach the range crest. Basins were each derived with standard hydrologic routing functions and hypsometry and hillslope angles (Figure 4) were measured directly from the topography and its derivative, respectively. Relief measurements, calculated as the difference between two elevations, are inherently subject to bias from the horizontal length scale between elevation measurements. Rather than measure mean relief over a fixed distance, which would primarily reflect mean hillslope angle, an alternative relief measure was devised to convey the degree of overall range dissection. This relief measurement, termed here as the internal relief, is defined as the maximum elevation difference among all elevation points equidistant from the basin outlet, e.g., the lowest and highest elevation among all the points that are 5 km from the outlet. Typical values of internal relief climb monotonically upstream from the basin outlet, hover around a maximum level in the middle basin reach, and descend towards the divide (Fig. 5). In practice, internal relief correlates to the product of basin area and mean hillslope angle, and therefore provides a measure of the ridge-to-valley relief that reveals how extensively glaciers and rivers have incised below adjacent peaks. Because extreme values of relief and elevation within Kyrgyz Range catchments tend to bias values toward isolated high peaks that occupy only a small fraction of the landscape, the upper quartile of internal relief and the lower, middle, and upper quartiles of elevation (as defined by the hypsometry) provide a better characterization of key topographic attributes (Fig. 4).

The distributions of hillslope angle, hypsometry, and internal relief from east to west within the Kyrgyz Range reveal a pattern of initial surface uplift followed by dissection and then stabilization

of range-scale morphology. At the easternmost end of the range (surface uplift zone on Fig. 4), the upper quartile of internal relief is < 600 m, the mean elevation is <3100 m, peak heights are <4000 m, and the range of hypsometry (measured by difference between the 1st and 3rd quartiles of the hypsometry) is <500 m. Low relief and a limited range of altitude indicate only limited dissection of this high mountain range and support predominance of surface uplift over erosion here. Moving westward, peak elevations, internal relief, and the range of hypsometry all continue to increase toward the center of the Kyrgyz Range (transition zone on Fig. 4), whereas the mean elevation remains nearly constant across this 80-km span. The increase in the elevation of the highest peaks suggests that total rock uplift increases toward the west. Similarly, the growth of internal relief and hypsometric range indicate increasing dissection across this tract. In this zone, adjacent basins compete to attain necessary size and gradients in order to balance rock uplift. Overall stability of morphologic indices along the central part of the range (steady morphology zone, Fig. 4) suggests that this region may have reached an equilibrium topographic form in which erosion by balances tectonic uplift.

Fission-track methodology

Apatite fission-track data from exhumed basement rocks often yield distinctive age-elevation patterns that can be used to infer the low-temperature exhumation history of a range. Samples may have been exhumed from sufficient depth during the most recent exhumation event that the maximum temperature, T_{max}, exceeded the total annealing temperature (Figure 6a). In this case, the fission-track clock was reset to zero, and fission-track data record information on the time-temperature cooling path of the sample as it cooled through the partial annealing zone (PAZ) during exhumation [e.g. *Green et al.*, 1989a, 1989b]. For apatites that are cooled moderately rapidly (10°C/Myr) and which have kinetic parameters similar to Durango apatite, the total annealing temperature is ~120°C [*Donelick et al.*, 1999; *Ketcham et al.*, 1999]. Samples in the rock

column above the total annealing isotherm experienced lower T_{max} prior to exhumation; these samples resided in the (now exhumed) PAZ for some period of time and therefore have ages reflecting the penultimate cooling event, (strongly) modified by partial annealing [e.g., *Fitzgerald et al.*, 1995] (Figure 6a). The age of the transition between these two suites of samples is interpreted to represent the onset of rapid exhumation.

The apatites analyzed in this study often have variable kinetic properties, as documented by both etch pit diameter (Dpar) and Cl content. These two methods have been shown to yield equally useful data for assessing the kinetic properties of apatite [*Donelick et al.*, 1999; *Ketcham et al.*, 1999]. In particular, apatites distinguished by large etch-pit diameters and high Cl content (herein termed "more resistant") are typified by higher annealing temperatures in contrast to less resistant apatites [e.g., *Green et al.*, 1989b; *Ketcham et al.*, 1999]. Given these contrasting annealing temperatures a superficial interpretation of an age-elevation plot can yield false conclusions about both the onset and rate of exhumation. Although the total annealing temperature of different apatite types is variable, the low temperature annealing behavior of apatites appears to be similar [*Ketcham et al.*, 1999]. Therefore, the slope of the exhumed partial annealing zone on an age-elevation plot for different apatite types cannot be assumed to be parallel (Figure 6). To avoid this pitfall, we have plotted age-elevation curves for apatites with similar kinetic properties. The long period of tectonic quiescence prior to the onset of Neogene exhumation implies a stable thermal structure in the upper crust [*Bullen et al.*, 2001]. Therefore, the slope of the age-elevation curve within the exhumed PAZ for kinetically similar apatites which have experienced similar thermal histories should be about the same for all of our profiles. This assumes that only a small, similar amount of horizontal-axis rotation has been experienced at each of the profiles located in the hanging wall of a major thrust. A contrasting age-elevation slope will pertain for apatites with differing kinetic characteristics (see Figure 6).

Sample preparation and analytical details are presented in Table 1. The young apatite samples yielded very few horizontal confined track-length measurements; up to 100 track-lengths were measured from older samples. For age determinations, 15 to 31 grains per sample were selected at random and dated; 1 sample yielded only 4 countable grains. Following convention, all statistical uncertainties on pooled ages and mean track lengths are quoted at the $\pm 1\sigma$ level, but $\pm 2\sigma$ uncertainties are taken into account for geologic interpretation. To assess the kinetic properties of apatite, four Dpar measurements were averaged from each dated crystal and from each crystal which yielded a confined track length, provided that sufficient etch pits were present. Dpar values are operator and etchant-dependent [*Sobel et. al.*, 2004]. Therefore, seven samples were also analyzed with a CAMECA SX-50 or SX-100 electron microprobe in order to determine Cl content (Table 1). Every crystal with a single grain age or a confined track-length measurement was probed. The microprobe data were used to calibrate the Dpar measurements.

In the context of age-elevation data, we utilize the AFT data from 3 transects to reconstruct the onset and rate of exhumation for each transect. Subsequently, Cenozoic burial and exhumation histories are evaluated using thermal models of higher elevation samples.

Results

Shamsi

Samples were collected along a tributary of the Shamsi river valley between 2250 and 3770 m along a transect that traverses a continuous sequence of Carboniferous quartzite from the base of the valley up to the crest of the east flanking ridge (Fig. 3).

The six samples yielded Miocene to Jurassic ages, generally increasing with elevation (Table 1; Figure 7. Four of them define a readily interpretable succession that captures the base of an exhumed partial annealing zone. These samples also illustrate the complications introduced by apparent mixtures of apatites with different annealing temperatures within the same bedrock

sample. With an age of 6.3 ± 0.8 Ma, the basal, youngest sample (TS164) passes the χ^2 test; all analyzed grains have similar kinetic properties as shown by Dpar (1.74 μm, SD 0.11) and microprobe (0.07 wt% Cl, SD 0.05) (Table 1; Figure DR1). The next sample (TS165) has a central age of 14 ± 7 Ma and fails the χ^2test. Eleven of the twelve countable grains form a young population, pass the χ^2test with a pooled age of 6.7 ± 1.8 Ma and a mean Dpar of 1.74 μm. A single grain has an age of 124 ± 44 Ma and a Dpar of 2.04 μm. However, microprobe data does not differentiate this grain; the average chlorine value of the sample is 0.12 wt% and the old grain has a value of 0.11 wt%. The third sample (TS166) passes the χ^2 test and has a pooled age of 17 ± 2 Ma and a Dpar value of 1.74 μm. The highest elevation sample (TS170) fails the χ^2test and has a central age of 91 ± 6 Ma, a Dpar value of 1.65 μm, and 0.12 wt%cl. However, one crystal has an anomalously high wt%cl of 0.45%; excluding this grain, the sample passes the χ^2test and has a pooled age of 88 ± 5 Ma and 0.07 wt%cl. For these latter two samples, there is no relationship between age and Dpar. Excluding the single old, high Dpar grain in sample TS165, these 4 samples can be plotted together on an age-elevation plot (Figure 7).

The lower two samples show rapid cooling, while the upper two show slow cooling within an exhumed PAZ. The inflection point between the two segments, at ~2800 m and 7 Ma, defines the onset of rapid cooling. Assuming that the sample experienced some amount of heating due to Miocene sedimentation prior to rapid exhumation, the total annealing temperature corresponding to the inflection point of this low Cl path is 100-105°C. Based on the age and elevation differences of these two partially reset samples, the apparent exhumation rate for the exhumed PAZ is about 12 ± 1 m/Myr (0.012 ± 0.001 km/Myr). This value will be used to define the apparent exhumation rate for the exhumed PAZ at Issyk Ata, because this section experienced a similar burial history (c.f, Fig. 6). As will be shown below, the corresponding rate at Boom Gorge is ca. 0.01 km/Myr, supporting this assumption. After 7 Ma, the rate at Shamsi accelerated to ~1 km/Myr.

Two additional samples lie within the exhumed PAZ. Both pass the chi-squared test. TS167 has an age of 67 ± 3 Ma, Dpar of 1.96 μm and 0.10 wt%Cl (0.08 wt%Cl excluding 5 grains with high values); TS169 has an age of 151 ± 6 Ma, Dpar of 2.04 and 0.26 wt%Cl (Table 1; Figure DR1). Because TS169 is significantly older than the two bounding samples TS167 and TS170, plotting all of the samples within the exhumed PAZ together cannot yield a readily interpretable age-elevation plot. However, placing kinetically different samples on subparallel trends reveals that more resistant apatites have consistently older ages, representing older portions of a single exhumed PAZ.

Issyk Ata

Samples were collected from a transect along the Issyk Ata river valley between 1840 and 3290 m. (Fig. 4). Nearby, glaciated peaks reach elevations of 4500 m. The transect samples primarily Late Ordovician granite; the second sample above the base is an apatite-poor Riphean metavolcanic rock.

Five of the six analyzed samples pass the chi-squared test, yielding ages ranging from 3.9 ± 0.7 Ma to 6.9 ± 0.6 Ma (Table 1; Figure 7). Four of these samples, Mav38, TS158, TS159, and TS162 appear to be monocompositional based on Dpar measurements and microprobe analysis. Dpar values are 1.65, 1.36, 1.87, and 1.92,respectively; the former sample yields a wt%Cl of 0.02 (Table 1; Figure DR1). Sample TS163 yielded only 4 countable grains; the resulting age is consistent with the other samples but of too low precision to warrant further attention. Sample TS161 contains two components that each pass the chi-squared test. A young population of 25 grains yields an age of 7.6 ± 1.9 Ma; an older component with 6 grains provides an age of 102 ± 11 Ma. The younger population has a Dpar of 1.72 μm and a wt%Cl of 0.02. Kinetic characteristics do not explain all of the grains in the older population: 5 of the 6 older grains yield higher values of 0.17 wt%Cl, whereas 1 grain has a value of 0.01 wt%Cl. Three of the old grains have large Dpar values of 2.43;

the other 3 fall within the cluster of young grains with an average value 1.83. When combined, the 6 grains have an average value of 2.13 μm.

The young, low resistant grains from these 6 samples define a steep linear trend on an age-elevation plot, indicating rapid cooling from below the base of an exhumed PAZ. The trend of the corresponding exhumed PAZ is assumed to have the same slope as the corresponding curve at Shamsi. Due to the absence of low resistance, partially reset samples, the position of this latter curve is poorly defined; hence, the onset of this rapid cooling can only be constrained as older than about 8 Ma. Using Fig. 6D as an analogy, the slope of the exhumed PAZ through the more resistant component of sample TS161 should have the same slope as the less resistant component; the two curves should be separated by a vertical distance corresponding to the difference in T_a for the two components. Although the more resistant slope is poorly constrained, this analysis suggests that the onset of rapid cooling should be represented by an elevation close to TS161 and hence only slightly older than 8 Ma.

Boom gorge

Two samples were collected from the Boom gorge along the Chu River at 1375 and 1530 m; these lie ca. 1500 m below the local peaks (Fig. 4). Both samples are from topographically low positions in the footwall of the main range-bounding thrust, in contrast to the hanging wall sections sampled at Shamsi and Issyk Ata. Cenozoic sediments lying above the regional erosion surface are preserved in the center of the range, overthrust by Paleozoic strata. The same sedimentary sequence lies north and south of the range, overthrust from the south and north, respectively. The Cenozoic strata in this region do not exceed 1.5 km in thickness [*Trofimov et al.*, 1976]. Sample TS84 was collected from a Permian granite just below the erosion surface; both the granite and the Cenozoic strata have been overthrust by Paleozoic units. Sample TS27 was collected from Devonian - Upper Carboniferous sandstone.

The two samples both pass the chi-squared test, with pooled ages of 128 ± 10 and 150 ± 8 Ma (Table 1; Figure 7). The older sample, TS84, has a Dpar of 1.70 μm (Table 1; Figure DR1). The younger sample, TS27, was prepared with slightly different etching conditions; therefore, Dpar was not measured. The samples yielded similar track-length data of 12.50 and 12.82 μm, respectively. The two samples lie on a cooling trend representing an exhumed PAZ; assuming that the two samples have the same kinetic characteristics, they experienced an apparent exhumation rate of 0.01 km/Myr. Because sample TS27 was collected from a structurally deep position within the Boom gorge, the amount of exhumation in the gorge is clearly limited.

Thermal modeling

Track-length modeling cannot determine a unique thermal history; rather, it yields a range of solutions which are consistent with the observed data. Thermal modeling combining track length, single crystal ages and weight percent chlorine were performed using the AFTSolve program [*Ketcham et al.*, 2000] and the annealing model of Ketcham et al. [1999]. This program determines the best-fit models as well as good and acceptable fits. Modeling of partially annealed samples provides good constraints on the total annealing temperature and the maximum Miocene burial temperature; the minimum temperature prior to Late Cenozoic burial is less well constrained. With information on the thermal state of the crust, this information delineates the depth of the sample below the regional erosion surface and the Late Cenozoic sediments that formerly overlay the area. The constraints on the time of final exhumation of partially annealed samples from modeling are often less precise; however, this information may be available from lower elevation samples in the same transect.

Converting thermal histories into exhumation paths requires information on the thermal state of the crust and, ideally, thermal conductivity. Borehole data suggest that the geothermal gradient within the study area is presently 25-30°C/km [*Gubin*, 1986]; herein, we use a value of 26°C

[*Shvartzman*, 1992]. Conductivity data are sparse. Exhumation rates are more difficult to calculate, given that one must also consider advection of isotherms due to thrusting [e.g., *Brown and Summerfield*, 1997; *Mancktelow and Grasemann*, 1997] and perturbations of isotherms due to topographic effects [e.g., *Stüwe et al.*, 1994]. In this study, neither factor likely had a significant effect, because there was almost no relief when exhumation began and there were only a few kilometers of rapid exhumation. As will be shown below, significant relief likely developed after the main phase of rapid exhumation had already set the fission-track ages.

Two of the Shamsi samples, TS167 and TS169, yielded sufficient track-length measurements to permit robust thermal modeling (Figure 8); however, given that TS169 yielded twice as many measurements, these results are considered more reliable. Both samples were modeled using four time-temperature constraints. Models were started at 250 Ma, with a temperature range between 70 and 160°C, such that all tracks initially formed could be completely annealed. The observed shortened track-length distributions require a late-stage heating event, consistent with burial heating due to the Oligo-Miocene depositional history discussed above. Three runs were made for each sample, with modeled reheating started at 30, 25, or 20 Ma. At this time, the model permitted sample temperatures between 25°C and 90°C, consistent with the samples being close to the paleo-surface. The peak reheating age of 7 Ma was set to match results from the vertical profile. The maximum reheating temperature was constrained to be between 30°C and 100°C. The final constraint was the present surface temperature of 10-20°C. Acceptable fits were not limited by the temperature or the position of the constraints, with the exception of the age of maximum reheating. Temperature paths between adjacent constraints had 8 segments. Heating and cooling rates were not constrained. Each model run had 10,000 iterations, using a Monte Carlo approach.

Several conclusions can be drawn from the modeling data (Figure 8 and Table 2). The influence of the Miocene sedimentary burial is significant; numerous model runs (not shown) which neglect this reheating did not produce good fits. The total annealing temperature (T_a)

depends on both apatite kinetic characteristics and cooling rate. T_a can be estimated as the best-fit temperature at which the oldest preserved track formed; the modeled temperatures can be verified by comparison with calculated temperatures reported by *Ketcham et al.* [1999]. Results from shallow samples can be used to understand the behavior of structurally deeper samples with similar kinetic characteristics because the temperature where and when the inflection point in the PAZ curve formed was approximately T_a. This position would have been buried beneath a column of bedrock and the Oligo-Miocene sedimentary basin.

The amount of Miocene reheating experienced by the samples provides a measure of the thickness of the Oligocene-Miocene sedimentary basin deposited prior to the onset of uplift of the Kyrgyz Range. From this reheating history, the thickness of the exhumed bedrock section and hence the subsurface position of the exhumed erosion surface can be estimated. Assuming a geothermal gradient of 26°C/km and based on the range of modeled heating of 18-34°C (Table 2) between 0.7 and 1.8 km of sediment was deposited at Shamsi. The broad range is partially due to the reduced sensitivity of the model at the low temperatures experienced prior to burial. Therefore, a more robust calculation taking into account the unsteady thermal conditions within a young sedimentary basin is inappropriate. However, the sedimentary thickness calculated is in agreement with geological observations from the Chu basin [*Chediya*, 1986; *Bullen et al.*, 2003].

AFTSolve modeling of sample TS84 from the Boom Gorge cannot precisely constrain the timing of final exhumation (Figure 8). The modeling strategy was similar to that used with the Shamsi samples, except that reheating began at 10, 15 or 20 Ma and final cooling began at 2, 3 or 5 Ma. Best-fit models suggests only 4-22°C of Neogene heating below the sedimentary basin; however, acceptable fits permit up to 32°C of heating, consistent with the up to 1.5 km of sediment preserved nearby.

Discussion

Multi-compositional age-elevation plots

Kinetically similar age-elevation curves at Shamsi and Issyk Ata represent an exhumed PAZ and are expected to have similar slopes, consistent with geological data that suggests that they have experienced similar thermal histories. However, curves within the same transect representing apatites with different resistances to annealing are often not parallel because both the T_a and the influence of Cenozoic burial heating are different. For instance, a more resistant apatite is reset at a lower elevation (higher temperature); at intermediate elevations, this apatite will display an older age than less resistant apatite because the former has experienced less annealing in the (now exhumed) PAZ (Figure 6A). In the case of a single large exhumation event, more resistant apatites should lie on a steeper trend within the PAZ. However, subsequent reheating due to burial beneath a sedimentary basin can partially reset this exhumed PAZ, creating a zone with a parallel trend (Fig. 6C). Subsequent exhumation can expose this history (Fig. 6D). In such a case, the transition from parallel to convergent paths in the exhumed PAZ marks the base of older exhumed PAZ. At Shamsi, this transition occurs 1 km above the base of the ultimate exhumed PAZ (Fig. 7). Making the simplifying assumptions that isotherms have not been perturbed and that the geothermal gradient has remained constant, and with independent information on the amount of burial, it is possible to estimate the magnitude of the older exhumation event (cf. Fig. 6D). If burial beneath the Chu basin was 1 to 1.5 km, this suggests that the magnitude of the exhumation event associated with creation of the Cretaceous erosion surface was 2 to 2.5 km. The range of old ages obtained from the Kyrgyz range and the adjacent Chu basin [this study; *Bullen et al.*, 2001] also implies that the penultimate exhumation event was not large enough to reset more thermally resistant all apatites.

Three-stage cooling history

Variable age-elevation slopes for kinetically dissimilar apatites support Oligo-Miocene burial followed by a three-stage cooling history for the Kyrgyz Range: (1) rapid cooling during removal of Cenozoic cover strata, (2) initially reduced erosion and cooling following exhumation of pre-Cenozoic bedrock, and (3) renewed rapid cooling and erosion into bedrock (Figure 9). This history is best defined by the Shamsi age-elevation curve. Only the lower portion of the Issyk Ata curve can presently be well defined with this cooling history. Although erosion has partially removed the AFT record of three-stage cooling at Ala Archa, it is also defined by U-Th/He dating of apatite there [*Bullen et al.*, 2003].

For Issyk Ata and Shamsi, the portion of the age-elevation plot below the inflection point yields apparent exhumation rates of ca. 0.4 and ca. 1 km/Myr, respectively. The ca. 1 to 1.5 km of sediment overlying the basement would require between 2 to 4 Myr and 1 to 1.5 Myr, respectively, to have been removed at these rates. For Shamsi, where the age and paleodepth of the inflection point is well constrained as 7 Ma and 4.0 to 4.6 km (Figure 7), the mean exhumation rate from this point to the surface is 0.6 to 0.7 km/Myr. This suggests that the rapid cooling recorded in the age-elevation profiles reflects the removal of the sedimentary section and that the exhumation rate decreased at least slightly afterwards. Similar conclusions about the magnitude of exhumation were reached by *Bullen et al.* [2003] for the Ala Archa section, based on both apatite fission-track and U-Th/He thermochronology. In particular, these authors concluded that a ca.1 Myr pulse of rapid exhumation at ~ 11-10 Ma removed 1.5 km of section at 1.0 to 1.5 km/Myr. Subsequently, the exhumation rate decreased to <0.3 km/Myr until 3 Ma, when the rate increased again to 0.8 km/Myr. These changes were similar in magnitude to synchronous changes in rates of shortening along the northern flank of the central Kyrgyz Range and rates of sediment accumulation in the Chu Basin [*Bullen et al.*, 2003] The fission-track data presented in this study cannot address whether the exhumation rate changed in the last several Myr at Issyk Ata or Shamsi.

The three-stage cooling pattern documented in the Kyrgyz range is likely to be broadly applicable. The typical geometry of a foreland-propagating thrust belt includes a foreland basin that is eventually disrupted by the advancing reverse-fault-front (Figure 9). In this setting, uplift above a new thrust or fold first exhumes the recently deposited sediment of the foreland basin. These sediments are typically poorly cemented and therefore easily eroded. Only when the vertical displacement of the fault exceeds the thickness of the overlying young sediment are older units exposed. Easily eroded, recently deposited sedimentary rocks can be rapidly exhumed with negligible surface uplift. As increasing amounts of resistant basement are exposed, exhumation rates decrease while surface uplift rates increase, if shortening rates remain steady [c.f., *Burbank et al.*, 1999; *Sobel and Strecker*, 2003]. Surface processes immediately respond to topographic relief developed by range growth and initiate drainage networks that can eventually bring erosion rates into balance with rock-uplift rates. Orographically enhanced precipitation and glacial erosion may further enhance the effectiveness of erosion as the range grows. At this point, if the time scale of geomorphic adjustment to range uplift is sufficiently rapid, range morphology may reach a steady state dictated by the interplay of surface processes and rock uplift.

Lateral propagation rate

The transition from slow cooling, followed by burial, to rapid cooling measures exhumation of the Kyrgyz Range via initial erosional stripping of Cenozoic cover strata at the onset of thrusting at the range tip. The best estimates for the onset of this rapid exhumation are 11 ± 1 Ma at Ala Archa [*Bullen et al.*, 2001] and 7 ± 0.5 Ma at Shamsi; these sections are 64 ± 7 km apart (Figure 7). The start of exhumation at Issyk Ata, located half-way between these locations, can only be constrained as slightly older than 8 Ma. Plotting initiation age versus distance east of Ala Archa shows that the range has propagated eastward at ca. 16 ± 6 km/Myr from 11 to 7 Ma.

Progressive changes in the geomorphology of basement rocks that form the easternmost Kyrgyz Range provides some independent constraint as to the relative rates of lateral propagation and uplift. As soon as rock uplift raises the Cenozoic sedimentary cover rocks above local base level, they appear to be rapidly stripped from above the pre-Cenozoic erosion surface and do not contribute significantly to the topography of the range. Topographic relief grows primarily within the pre-Cenozoic bedrock via surface uplift that results from the competition between rock uplift and exhumation. The abrupt increases in mean and maximum basin elevation in the surface uplift zone with only nominal gain of internal relief suggests that the form of the nascent range near its terminus is dictated primarily by rock uplift above the south-dipping thrust fault, that peak heights are correlated with the magnitude of fault slip, and that the magnitude of dissection is minimal. The gradient of peak elevations in the surface uplift zone define an east-west slope of 13% ± 2% (Fig. 4), which, if built by thrusting at a uniform slip rate and without significant erosion of the peaks, corresponds to a lateral propagation rate that is only 7 to 9 times the rock uplift rate. Such a gradient could not have applied over the entire interval of range growth, however, because it would require over 15 km of rock uplift in the central part of the range: an amount inconsistent with the Ala Archa fission-track data. Hence, the propagation/rock-uplift ratio appears considerably lower near the eastern tip of the range than it does farther west. A quasi-elliptical distribution of fault slip, similar to that documented for propagating normal faults [*Dawers*, 1993], could be responsible for a steeper rock-uplift gradient on the presently propagating easternmost tip of the Kyrgyz Range than that derived from Miocene exhumation of the central part of the range. Alternatively, a diminished lateral propagation rate could have arose in response to structural interference [*Gupta and Scholz, 2000*] with reverse faults and strike-slip faults emerging from the Kungey Alatoo to the northeast. Independent geochronological constraints of either fault slip rate or the ages of initiation of glaciation in the easternmost Kyrgyz Range as rocks were uplifted above the glacial ELA could test these predictions.

Geomorphic adjustment to bedrock uplift

The geomorphic evolution of the Kyrgyz Range supports progressive adjustment of surface uplift and incision in response to rock uplift. At the easternmost propagating tip of the Kyrgyz Range, limited dissection of the pre-Cenozoic erosion surface enhances surface uplift and dampens internal relief. This contrasts with the steady morphology zone in the central part of the range (Fig. 4) where the pre-Cenozoic erosion surface has been completely removed and large north-facing basins with > 1000 m of internal relief predominate. Given the north-vergent underlying thrust faults and the structural culmination along the northern edge of the range, the observation that the south-facing basins are significantly smaller than the north-facing basins suggests that the northern basins have grown at the expense of south-facing ones. This southward migration of the drainage divide results in a drainage asymmetry that is opposite to that expected for ranges developed above a (singular) actively deforming structure, wherein the steep limb or flank with shorter catchments lies above the active fault [*Leeder and Jackson*, 1993; *Talling*, 1997; *Burbank and Anderson*, 2001]. However, this observation is consistent with both range asymmetry driven by > 1000 m lower base-level on its north side [*Ellis and Densmore*, 2003] and with the higher precipitation received on the north flank of the range [*Aizen et al.*, 1995].

The transition zone, which lies between the zone of surface uplift and the zone of steady morphology, provides important insight into the transformation of the Kyrgyz Range by surface processes. Peak heights increase gradually from east to west within the transition zone, albeit at a much more gentle gradient than in the eastern surface-uplift zone, because of greater competition between rock uplift and erosion. The most striking aspect of the transition zone is that mean elevation attains a near-constant value of ~3200 m despite ongoing growth of peak heights, range of hypsometry, and internal relief (Fig. 4). Systematic increase of north-facing basin size explains these contradictory elevation and relief trends. The first significant enlargement of north-facing

basins occurs where peak elevations exceed 3500 m elevation above mean sea level (Fig. 4), enabling Pleistocene glaciation of the range crest to lengthen north-facing basins southward via cirque retreat (Figs. 3 and 5), [*Oskin and Burbank, submitted manuscript*]. Internal relief increases only modestly within these glacially expanded north-facing catchments because glacial erosion is limited to high elevations. Consequently, hypsometry remains concentrated near the glacial ELA [c.f. *Brozovic et al.*, 1997]. Further west within the transition zone, expansion of north-facing basins eventually leads to more effective fluvial and glacial erosion at lower elevations, which in turn causes the range of hypsometry to expand and internal relief to grow to >1500m. In the westernmost transition zone, the internal relief attains its maximum as rivers in deeply incised valleys abut against hillslopes that are at or near the threshold angle for failure. Overall, the transition zone appears to be a region of stabilization of elevation, if not locally even of surface depression, as large north-facing basins enlarge and mature.

Coupled Exhumation and Shortening

Structural reconstructions of the central Kyrgyz Range [*Bullen et al.*, 2003] suggest the pattern of shortening may be correlated to the exhumation rate. Initial, rapid shortening corresponds to high cooling rates during removal of Cenozoic cover rocks from the crest of the range. This was followed by a period of slow shortening rate and backthrusting within the foreland basin, north of the Kyrgyz Range, corresponding to a period of slow exhumation of Paleozoic bedrock. In the past 3 Myr, both shortening rate and exhumation of the bedrock core have increased. If the exhumation history of the Kyrgyz Range is driven by the interplay of rock erodability with both rock and surface uplift, then this correlation could indicate a feedback mechanism whereby exhumation rates are reduced when more resistant rocks are at the surface, thereby building topography. To the extent that larger topographic loads require more work for a given increment of shortening and rock uplift, shortening and both rock- and surface uplift rates may diminish as topography grows and the

locus of deformation shifts elsewhere in the range [e.g., *Masek and Duncan*, 1998]. If erosion in a given range is inefficient and its topography grows, the increased load may cause shortening rates to diminish or deformation to shift entirely to a site requiring less work. This model predicts variations in exhumation rate with time driven by changes in erosion parameters; the evidence of this behavior should be detectable both in the cooling history of the range and in the depositional history of the adjacent basin. If the Kyrgyz Range has continued to evolve in a similar manner to that expressed in the bedrock and detrital cooling history [*Bullen et al., 2003*], then the along-strike geomorphic evolution of the range should also be consistent with the proposed exhumation model. Here we explore the plausibility of coupling between surface uplift and shortening rate at the range scale.

In the Kyrgyz Range, a short pulse of rapid cooling at several sites is associated with 1 to 1.5 km of exhumation; this thickness corresponds well with the thickness of the young sedimentary basin which formerly overlay the range. Therefore, most of this pulse of rapid cooling is probably attributable to the removal of this sediment during the initial phase of rock uplift. Because the young sedimentary rocks are more easily eroded than the underlying Paleozoic units, this short episode of rapid cooling likely corresponded to only a small amount of surface uplift [*Bullen et al., 2003*]. Only when a significant amount of bedrock was exposed could the surface uplift increase and the concurrent exhumation rate decrease. This pattern is seen in the geomorphology of the surface uplift zone of the Kyrgyz Range, where easily eroded Cenozoic rocks are rapidly removed from the range but the underlying pre-Cenozoic unconformity surface is widely preserved up to high elevations. The observation that an initial pulse of rapid exhumation propagates along the strike of the range, roughly normal to the principal shortening direction, suggests that the range is growing due to lengthening of the bounding structure rather than due to changes in the regional stress field.

Bullen et al. [2003] suggested that the decrease in exhumation rate at ca. 10 Ma at Ala Archa was associated with the observed decrease in range-normal shortening rate and with a shift from thrusting to backthrusting. We further suggest that, as the range-bounding thrust fault lengthened, this deformation pattern likely propagated along the strike of the range in the same manner. Basinward propagating foreland thrust faults and folds, including prominent backthrusts, are observed along the length of the range east from Ala Archa. We deduce from the thermal history of lateral range propagation that these foreland faults have also propagated eastward as the range itself propagated.. Such a spatially varying decrease in shortening rate, if supported from the history of these foreland structures, would suggest a feedback between the size of the range and the activity of the basal thrust and growing topography [cf. *Davis et al.* 1983]. We speculate that the geomorphic transition zone is the surficial expression of a coupled deformation-erosion system that is out of balance, leading to a feedback between erosional efficiency and the locus of deformation.

Steady state time scale

Consistency between the cooling history and the along-strike geomorphic evolution of the Kyrgyz Range supports the hypothesis that exhumation rate, and possibly also shortening rate, are modulated by the time scale of adjustment of surface processes to rock uplift. No single steady state time scale adequately describes the variety and significance of adjustments toward steady morphology in the Kyrgyz Range. Erosion is immediately effective at stripping the cover from the pre-Cenozoic erosion surface, supporting an initial, short adjustment time of less than 1 Myr for steady state rock uplift and erosion of Cenozoic strata. Conversely, significantly longer time periods are necessary for erosion to balance rock uplift of resistant Paleozoic basement. In the surface uplift zone, below the elevation of glacial ice accumulation, surface processes fail to substantively alter the structural form of the range. Low elevation ranges of the western Tien Shan commonly preserve extensive areas of the pre-Cenozoic erosion surface [*Abdrakmatov et al.*,

2001], indicating that the steady state time scale in the absence of glaciation is longer than the time since Early to Mid Miocene onset of uplift. Glaciation of the easternmost Kyrgyz Range triggers the first significant erosional response to rock uplift via establishing, lengthening, and incising canyons. Formation of internal relief here corresponds to a sharp decrease in mean basin hypsometry and increasing mean hillslope angles as glacio-fluvial erosion counterbalances, and even temporarily exceeds, rock uplift. Over 80% of the adjustment of hypsometry, peak elevations, internal relief, and mean slope angles occurs by within the first 25 km of the transition zone, suggesting that a quasi-steady state is reached within 2 to 3 Myr after the onset of glaciation and canyon cutting in the surface uplift zone. The complete transition to a steady morphology occurs gradually and cannot be defined by a sharp break in morphometric indices at the end of the transition zone. Mean hypsometry is steady between 3000 and 3500 m for all points west of the surface uplift zone. Mean slope angle levels off gradually west of Shamsi, and internal relief climbs to maximum values west of Issyk Ata. Overall, approximately 110 km of the east Kyrgyz Range shows evidence for dynamic adjustment of its geomorphology to balance erosion and rock uplift. This probably represents over 10 Myr of range propagation, and suggests that the time scale of geomorphic adjustment over active basement-cored uplifts of the Tien Shan spans back into Late Miocene time – a significant proportion of the total Cenozoic history of the northern Tien Shan.

In actively deforming the mountain ranges, the time to steady state is likely to be dependent on the efficiency of surface processes and the rates of deformation. Rapid rock-uplift rates tend to generate steep hillslopes and rivers, thereby accelerating erosion rates. Numerical models suggest that topographic steady state can be attained in <1 Myr where rates of deformation and erosion are high (equivalent to several mm/yr: Willett, 1999). Not surprisingly, in the Kyrgyz Range where rates are commonly ≤ 1 mm/yr, a longer interval is expected to be required to attain steady state.

Conclusions

Comparisons between exhumation histories derived from apatite fission-track analysis and the geomorphic evolution based on quantitative DEM analysis of the Kyrgyz Range permits a reconstruction of the entire 11Myr evolution of the range. Exhumation of the range commenced at ca. 11 Ma in the vicinity of Ala Archa and has propagated eastward. The lateral propogation rate between Ala Archa and Shamsi is ca. 16±6 km/Myr from 11 Ma to 7 Ma, and this rate has likely slowed as the range propagated farther eastward towards the Kungey Alatoo. Initial rock uplift leads to rapid stripping of poorly consolidated, young sediments; rapid exhumation (almost) balances rock uplift, creating only limited surface uplift. The ca. 1.5 km-thick portion of the Chu basin which formerly overlay the range above the Cretaceous erosion surface was stripped away in 1 to 2 Myr, corresponding to the brief episode of rapid cooling documented by apatite fission-track analysis and by the zone of surface uplift defined by the presence of the regional erosion surface. Once significant amounts of more resistant basement are exposed, the exhumation rate would be expected to decrease and surface uplift rate to increase if range-normal shortening rates were maintained. However, independent data suggests that the shortening rate actually decreased, suggesting that a feedback exists between erosional efficiency and the location and magnitude of shortening. In this transition zone, drainage networks propagate into the growing range, eventually bringing erosion rates into balance with rock-uplift rates. The timescale for the majority of this geomorphic adjustment is ca. 2 to 3 Myr after uplift of the range crest through the glacial ELA and development of glacially lengthened and incised canyons, However, additional systematic adjustments to mean slope angle, hypsometry, and internal relief occur before the transition to steady morphology is complete. Overall, the evolution of the Kyrgyz Range supports a model of a systematically time-varying exhumation and shortening rates that are modulated by changes in rock erodability, the efficiency of erosion processes, and the time scale of geomorphic adjustment to surface uplift.

Acknowledgements

Dieter Rhede and Oona Appelt helped collect the electron microprobe data. Mike Bullen kindly provided unpublished apatite kinetic data from the Ala Archa section. AM acknowledges support from the DAAD. Partial funding was provided by NASA (NAG5-9039; 10520).

References

Abbott, L.D., E.A. Silver, R.S. Anderson, R.B. Smith, J.C. Ingle, S.A. Kling, D. Haig, E. Small, J. Galewsky, and W. Sliter, Measurement of the tectonic uplift rate in a young collisional mountain belt, Finisterre Range, Papua New Guinea, *Nature*, *385*, 501-507, 1997.

Abdrakhmatov, K.E., R. Weldon, S. Thompson, D. Burbank, C. Rubin, M. Miller, and P. Molnar, Origin, direction, and rate of modern compression in the central Tien Shan, Kyrgyzstan, *Geologiya I Geofizika (Russian Geology and Geophysics)*, *42*, 1585-1609, 2001.

Abdrakhmatov, K.Y., S.A. Aldazhanov, B.H. Hager, M.W. Hamburger, T.A. Herring, K.B. Kalabaev, K.B. Kalabayev, V.I. Makarov, P. Molnar, S.V. Panasyuk, M.T. Prilepin, R.E. Reilinger, I.S. Sadybakasov, B.J. Souter, Y.A. Trapeznikov, V.Y. Tsurkov, and A.V. Zubovich, Relatively recent construction of the Tien Shan inferred from GPS measurements of present-day crustal deformation rates, *Nature*, *384* (6608), 450-453, 1996.

Ahnert, F., Functional relationships between denudation, relief, and uplift in large mid-latitude basins, *American Journal of Science*, *268*, 243-263, 1970.

Aizen, V.B., E.M. Aizen, and J.M. Melack, Climate, snow cover, glaciers, and runoff in the Tien Shan, Central Asia, *Water Resources Bulletin*, *31* (6), 1113-1129, 1995.

Bazhenov, M.L., A.Q. Collins, K.E. Degtyarev, N.M. Levashova, A.V. Mikolaichuk, V.E. Pavlov, and R. Van der Voo, Paleozoic northward drift of the North Tien Shan (Central Asia) as revealed by Ordovician and Carboniferous paleomagnetism, *Tectonophysics*, *366*, 113 – 141, 2003.

Bazhenov, M.L., V.S. Burtman, and A.V. Dvorova, Permian paleomagnetism of the Tien Shan fold belt, Central Asia: post-collisional rotations and deformation, *Tectonophysics*, *312* (2-4), 303-329, 1999.

Brown, R.W., and M.A. Summerfield, Some uncertainties in the derivation of rates of denudation from thermochronologic data, *Earth Surface Processes and Landforms*, *22* (3), 239-248, 1997.

Brozovic, N., D.W. Burbank, and A.J. Meigs, Climatic limits on landscape development in the northwestern Himalaya, *Science*, *276*, 571-574, 1997.

Bullen, M.E., D.W. Burbank, and J.I. Garver, Building the Northern Tien Shan: Integrated thermal, structural, and topographic constraints, *Journal of Geology*, *111* (2), 149-165, 2003.

Bullen, M.E., D.W. Burbank, J.I. Garver, and K.Y. Abdrakhmatov, Late Cenozoic tectonic evolution of the northwestern Tien Shan: New age estimates for the initiation of mountain building, *Geological Society of America Bulletin*, *113* (12), 1544-1559, 2001.

Bune, V.I., and G.P. Gorshkov, Seismic zoning territory of the USSR. Methodical bases and the regional description of the map of 1978 year [Seismicheskoe rayonirovanie territorii SSSR. Metodicheskie osnovy I regionalnoe opisanie karty 1978 goda] (In Russian), pp. 306, Nauka, Moscow, 1980.

Burbank, D., A. Meigs, and N. Brozovic, Interactions of growing folds and coeval depositional systems, *Basin Research*, *8*, 199-223, 1996.

Burbank, D.W., and R.S. Anderson, *Tectonic Geomorphology*, 273 pp., Blackwell Science, Malden, MA, 2001.

Burbank, D.W., J.K. McLean, M. Bullen, K.Y. Abdrakhmatov, and M.M. Miller, Partitioning of intermontane basins by thrust-related folding, Tien Shan, Kyrgyzstan, *Basin research*, *11* (1), 1999.

Burg, J.-P., A.V. Mikolaichuk, and F.Ch. Apayarov,(editors), Digital Geological Map of the Kyrgyz Range and Chu Basin Transitional Zone, SNF, Project No 7KSPJ065518, http://www.kyrgyzstan.ethz.ch, Zurich, 2004.

Burtman, V.S., Structural geology of Variscan Tien Shan, USSR, *American Journal of Science*, *275-A*, 157-186, 1975.

Carroll, A.R., S.A. Graham, E. Chang, and C.L. McKnight, Sinian through Permian tectonostratigraphic evolution of the northwestern Tarim basin, China, in *Paleozoic and*

Mesozoic tectonic evolution of central and eastern Asia: From continental assembly to intracontinental deformation, Memoir, Vol. 194, edited by M.S. Hendrix, and G.A. Davis, pp. 47-70, Geological Society of America, Boulder, 2001.

Cartwright, J.A., B.D. Trudgill, and C.S. Manfeld, Fault growth by segment linkage Ãn explanation for scatter in maximum displacement and trace length data from the Canyonlands grabens of SE Utah, *Journal of Structural Geology, 17*, 1319-1326, 1995.

Chediya, O.K., K.Y. Abdrakhmatov, I.H. Lamzin, G. Michel, and V. Michailev, Seismotectonic characterization of the Issyk Ata fault, pp. 58–69, Institute Nauk Kyrgyzskoi, Bishkek, 1998.

Chediya, O.K., *Morfostruktury i noveishii tektogenez Tyan'-Shanya (Morfostructures and Neotectonics of the Tien Shan)*, 314 pp., Ilim, Frunze, 1986.

Chediya, O.K., V.M. Yazovskii, and A.B. Fortuna, O stratigraficheskom raschlenenii krasnotsvetnogo kompleksa v Chuyskoy vpadine I yeye gornom obramlenii (The stratigraphic subdivision of the Kyrgyz red-bed complex in the Chu basin and the surrounding mountains), in *Zakonomernosti geologicheskogo razvitiya Tyan-Shanya v kaynozoye (Principles of the geologic development of the Tyan-Shan in the Cenozoi)*, pp. 26–52, Ilim, Bishkek, 1973.

Cobbold, P.R., E. Sadybakasov, and J.C. Thomas, Cenozoic transpression and basin development, Kyrgyz Tien Shan, central Asia, in *Geodynamic Evolution of Sedimentary Basins*, edited by F. Roure, N. Ellouz, V.S. Shein, and I. Skvortsov, pp. 181-202, Editions Technip, Paris, 1996.

Dawers, N.H., M.H. Anders, and C.H. Scholz, Growth of normal faults: Displacement-length scaling, *Geology, 21*, 1107-1110, 1993.

Donelick, R.A., R.A. Ketcham, and W.D. Carlson, Variability of apatite fission-track annealing kinetics: II. Crystallographic orientation effects, *American Mineralogist, 84* (9), 1224-1234, 1999.

Dumitru, T.A., A new computer automated microscope stage system for fission track analysis, *Nuclear tracks, 21* (4), 575-580, 1993.

Dumitru, T.A., D. Zhou, E.Z. Chang, S.A. Graham, M.S. Hendrix, E.R. Sobel, and A.R. Carroll, Uplift, exhumation, and deformation in the Chinese Tian Shan, in *Paleozoic and Mesozoic tectonic evolution of central and eastern Asia: From continental assembly to intracontinental deformation*, Memoir, Vol. 194, edited by M.S. Hendrix, and G.A. Davis, pp. 71-99, Geological Society of America, Boulder, 2001.

England, P.C., and P. Molnar, Surface uplift, uplift of rocks, and exhumation of rocks, *Geology, 18* (12), 1173-1177, 1990.

Erslev, E.A., Basement balancing of Rocky Mountain foreland uplifts, *Geology, 14*, 259-262, 1986.

Fitzgerald, P.G., R.B. Sorkhabi, T.F. Redfield, and E. Stump, Uplift and denudation of the central Alaska Range; a case study in the use of apatite fission track thermochronology to determine absolute uplift parameters, *Journal of Geophysical Research, 100* (10), 20,175-20,191, 1995.

Fortuna, A.B., C.K. Kerimbekov, S.I. Kyzikov, and A.V. Mikolaichuk, Lithostratigraphic and palynologic data of Cenozoic deposits of Tessik–Sarybulak depression, in *Geology of Cenozoic and Seismotectonics of the Tien Shan*, pp. 26–39, Ilim, Bishkek, 1994.

Green, P.F., I.R. Duddy, A.J.W. Gleadow, and J.F. Lovering, Apatite fission-track analysis as a paleotemperature indicator for hydrocarbon exploration, in *Thermal History of Sedimentary Basins: Methods and Case Histories*, edited by N.D. Naeser, and T.H. McCulloh, pp. 181-195, Springer-Verlag, New York, 1989.

Green, P.F., I.R. Duddy, G.M. Laslett, K.A. Hegarty, A.J.W. Gleadow, and J.F. Lovering, Thermal annealing of fission tracks in apatite, 4, Quantitative modelling techniques and extension to geological timescales, *Chem. Geol. (Isotope Geosci. Sec.), 79*, 155-182, 1989.

Gubin, I.E., *Lithosphere of Tien Shan*, 158 pp., Nauka, Moscow, 1986.

Gupta, A., and C. Scholz, A model of normal fault interaction based on observations and theory, *Journal of Structural Geology, 22*, 865-879, 2000.

Hallet, B., L. Hunter, and J. Bogen, Rates of erosion and sediment evacuation by glaciers: a review of field data and their implications, *Global Planetary Change*, *12*, 213-235, 1996.

Hendrix, M.S., S.A. Graham, A.R. Carroll, E.R. Sobel, C.L. McKnight, B.J. Schulein, and Z. Wang, Sedimentary record and climatic implications of recurrent deformation in the Tian Shan: Evidence from Mesozoic strata of the north Tarim, south Junggar, and Turpan basins, Northwest China, *Geological Society of America Bulletin*, *104* (1), 53-79, 1992.

Howard, A.D., A detachment-limited model of drainage basin evolution, *Water Resources Research*, *30*, 2261-2285, 1994.

Howard, A.D., and G. Kerby, Channel changes in badlands, *Geological Society of America Bulletin*, *94*, 739-752, 1983.

Hurford, A.J., and P.F. Green, The zeta age calibration of fission-track dating, *Chemical Geology*, *41* (4), 285-317, 1983.

Ketcham, R.A., R.A. Donelick, and M.B. Donelick, AFTSolve: A program for multi-kinetic modeling of apatite fission-track data, *Geological Materials Research*, *2* (1), 1-32, 2000.

Ketcham, R.A., R.A. Donelick, and W.D. Carlson, Variability of apatite fission-track annealing kinetics: III. Extrapolation to geological time scales, *American Mineralogist*, *84* (9), 1235-1255, 1999.

Kooi, H., and C. Beaumont, Large-scale geomorphology: classical concepts reconciled and integrated with contemporary ideas via a surface processes model, *Journal of Geophysical Research*, *101*, 3361-3386, 1996.

Krilov, A.Y., Absolute age of the rocks of the Central Tien Shan and application of Argon methods to metamorphic and sedimentary sediments, in *Determination of the Absolute Age of Pre-Quaternary Formations*, edited by I.E. Starik, pp. 222-224, Nedra, Moscow, 1960.

Leeder, M., R., and J.A. Jackson, The interaction between normal faulting and drainage in active extensional basins, with examples from the western United States and central Greece, *Basin Research, 5*, 79-102, 1993.

Makarov, V.I., *New tectonic structure of the Central Tien Shan*, 172 pp., Nauka, Moscow, 1977.

Mancktelow, N.S., and B. Grasemann, Time-dependent effects of heat advection and topography on cooling histories during erosion, *Tectonophysics, 270*, 167-195, 1997.

Masek, J.G., and C.C. Duncan, Minimum-work mountain building, *Journal of Geophysical Research, 103*, 907-917, 1998.

Mikolaichuk, A., E. Sobel, M. Gubrenko, and A. Lobanchenko, Structural Evolution of the Tien Shan Orogenic Northern Margin, *Proceedings of the National Academy of Sciences of Kyrgyz Republic, 4*, 50-58, 2003.

Mikolaichuk, A.V., The structural position of thrusts in the recent orogen of the Central Tien Shan, *Russian Geology and Geophysics, 41* (7), 961 - 970, 2000.

Oskin, M., and D.W. Burbank, Alpine landscape evolution dominated by cirque retreat, *Geology*, in review.

Reigber, C., G.W. Michel, R. Galas, D. Angermann, J. Klotz, J.Y. Chen, A. Papschev, R. Arslanov, V.E. Tzurkov, and M.C. Ishanov, New space geodetic constraints on the distribution of deformation in Central Asia, *Earth and Planetary Science Letters, 191* (1-2), 157-165, 2001.

Royden, L., Coupling and decoupling of crust and mantle in convergent orogens: Implications for strain partitioning in the crust, *Journal of Geophysical Research, 101* (B8), 17679-17705, 1996.

Sadybakasov, I.S., *Neotektonika Vysokoi Azii (Neotectonics of the High Asia)*, 181 pp., Nauka, Moscow, 1990.

Schmidt, K.M., and D.R. Montgomery, Rock mass strength assessment for bedrock landsliding, *Environmental & Engineering Geoscience, 2* (325-338), 1996.

Shvartzman, Y.G., Thermal field, seismicity and geodynamics of the Tien Shan, Unpub. Ph.D. dissertation thesis, University of Kyrgyzstan, Bishkek, 1992.

Sklar, L.S., and W.E. Dietrich, Sediment and rock strength controls on river incision into bedrock, *Geology*, *29*, 1087-1090, 2001.

Sobel, E., A. Mikolaichuk, J. Chen, and D. Burbank, Development of the Late Cenozoic Central Tian Shan in Kyrgyzstan and China Recorded by Apatite Fission Track Thermochronology, in *AGU Fall meeting*, pp. F1156, 2000.

Sobel, E.R., and M.R. Strecker, Uplift, exhumation, and precipitation: Tectonic and climatic control of Late Cenozoic landscape evolution in the northern Sierras Pampeanas, Argentina, *Basin Research*, *15*, doi: 10.1046/j.1365-2117.2003.00214.x, 2003.

Sobel, E.R., and T.A. Dumitru, Exhumation of the margins of the western Tarim basin during the Himalayan orogeny, *Journal of Geophysical Research*, *102* (B3), 5043-5064, 1997.

Sobel, E.R., Basin analysis of the Jurassic - Lower Cretaceous southwest Tarim basin, NW China, *Geological Society of America Bulletin*, *111* (5), 709-724, 1999.

Sobel, E.R., D. Seward, G. Ruiz, A. Kuonov, H. Ege, M. Wipf, and C. Krugh, Influence of Etching Conditions on Dpar Measurements: Implications for Thermal Modeling, in *International Fission Track Workshop*, Amsterdam, 2004.

SRTM, 2003

Stock, J.D., and D.R. Montgomery, Geologic constraints on bedrock river incision using the stream power law, *Journal of Geophysical Research-Solid Earth*, *104* (B3), 4983-4993, 1999.

Stüwe, K., L. White, and R. Brown, The influence of eroding topography on steady-state isotherms; application to fission track analysis, *Earth and Planetary Science Letters*, *124* (1-4), 63-74, 1994.

Talling, P.J., M.D. Stewart, C.P. Stark, S. Gupta, and S.J. Vincent, Regular spacing of drainage outlets from linear fault-blocks, *Basin Research*, *9*, 275-302, 1997.

Thompson, S.C., R.J. Weldon, C.M. Rubin, K. Abdrakhmatov, P. Molnar, and G.W. Berger, Late Quaternary slip rates across the central Tien Shan, Kyrgyzstan, central Asia, *Journal of Geophysical Research-Solid Earth, 107* (B9), 2002.

Trofimov, A.K., N.F. Udalov, N.G. Utkina, F.B. Fortuna, O.K. Chediya, and V.M. Yazovskii, *Geologiya kainozoya Chuiskoi vpadiny i ee gornogo obramleniya (Cenozoic Geology of the Chu Depression and Its Mountainous Surroundings)*, 128 pp., Nauka, Leningrad, 1976.

Whipple, K.X., and G.E. Tucker, Dynamics of the stream-power river incision model: Implications for height limits of mountain ranges, landscape response timescales, and research needs, *Journal of Geophysical Research-Solid Earth, 104* (B8), 17661-17674, 1999.

Whipple, K.X., Bedrock rivers and the geomorphology of active orogens, *Ann. Rev. Earth Planet. Sci., 32*, 151-185, 2004.

Willett, S.D., and M.T. Brandon, On steady states in mountain belts, *Geology, 30* (2), 175-178, 2002.

Willett, S.D., Orogeny and orography: The effects of erosion on the structure of mountain belts, *Journal of Geophysical Research-Solid Earth, 104* (B12), 28957-28981, 1999.

Yin, A., S. Nie, P. Craig, T.M. Harrison, F.J. Ryerson, X.L. Qian, and G. Yang, Late Cenozoic tectonic evolution of the southern Chinese Tian Shan, *Tectonics, 17* (1), 1-27, 1998.

Zhang, P., P. Molnar, and W.R. Downs, Increased sedimentation rates and grain sizes 2–4 Myr ago due to the influence of climate change on erosion rates, *Nature, 410*, 891-897, 2001.

Figures:

Figure 1. A. Topographic map of central Asia, showing locations of the Tien Shan with respect to adjacent plateaus and basins. The Kyrgyz Range forms the northern margin of the central Tien Shan. B. Topography of the Kyrgyz Range derived from 3 arcsec digital elevation model [*SRTM*, 2003]. Darker shades correspond to lower topography. Locations of apatite fission track (FT) samples from ***Bullen et al.*** [2001; 2003] and this study shown. Irregular outline defines east half of range analyzed in C and in Figure 4. C. Mean slope angle, mean elevation, and maximum elevation of the east half of the Kyrgyz Range measured in 10 km-wide swaths. Arrows point to area of analysis of B contained within white outline.

Figure 2. Map of the Kyrgyz range and adjacent basins, modified from *Mikolaichuk et al.* [2003]. Isopachs show depth to basement; Cenozoic strata of the Chu basin constitutes the majority of this sediment. The ranges are composed of Paleozoic units; Mesozoic units are virtually absent.

Figure 3. Shaded relief image and map of exhumed pre-Cenozoic erosion surface remnants of the easternmost Kyrgyz Range. Darker patches are mapped surface remnants with average southward dip shown in degrees. Lighter patches show extent of late Pleistocene glaciation shown. Reverse fault system bounds northern edge of range. Ages and sample locations from Shamsi River transect show complete exhumation of apatite fission-track partial annealing zone northwest of tilted erosion surface outcrops.

Figure 4. A. Topographic characteristics of north-facing basins along the length of the Kyrgyz range. Measured basins are shown directly below in B. Peak heights are highest elevations at the edge of each basin. Hypsometry shows median elevation bounded by 75^{th} and 25^{th} percentile

elevations. The difference between these is the hypsometric range, shown shaded as medium grey. Internal relief is measured as the difference between the highest and lowest elevations that are the same distance upstream from the basin outlet. The 75^{th} percentile of the distribution of internal relief within each basin plotted with area beneath this curve shaded dark grey. Surface uplift zone shows sharp increase in peak elevation, hypsometry, and internal relief from east to west in proportion to structural growth of the Kyrgyz Range. Adjustment zone shows progressive increases in mean slope angle, hypsometric range, and internal relief as north-facing basins expand and incise uplifted bedrock. These same morphometric indices are constant in the steady morphology zone.

Figure 5. Examples of progressive expansion and deepening of north facing basins. Komorchek lies at the transition from the surface uplift to the adjustment zone; Tchuk lies within the adjustment zone; Ala Archa lies within the steady morphology zone. Erosion from Komorchek to Tchuk is dominated by southward expansion of basins, probably via glacial cirque retreat. Prominent convexity in stream profile at Tchuk is a result of insufficient fluvial erosion downstream of glacially expanded valley. Erosion from Tchuk to Ala Archa dominated by removal of convexity by fluvial and glacial incision. Internal relief shown graphically as the shaded region between river longitudinal profile and equidistant ridge line elevations, where distance is measured up main and tributary streams to the divide. Internal relief effectively captures deepening of basins in adjustment zone.

Figure 6. Schematic illustration of the affect of differing total annealing temperatures (T_a) on complex cooling paths. The 4 vertical elevation profiles (A to D) represent a sequence of exhumation (cooling) and burial (reheating) events. The upper panel of each pair shows the evolving temperature history; the lower panel represents the distribution of apatite fission-track ages in a vertical profile at the corresponding time step. Each profile shows the cooling path of

apatites that are more (solid line) and less (dashed line) resistant to annealing. The base of the partial annealing zone (PAZ) for each type of apatite is considered to be the respective T_a. Exhumation and burial events are (unrealistically) depicted as instantaneous for clarity. The geothermal gradient is assumed to remain constant and advection of isotherms is neglected for simplicity.

A. A large deformation event followed by a long period of quiescence gives shallow samples a common age. More resistant apatites are reset at lower elevation (hotter temperature); therefore, the slope of the more resistant cooling path is steeper in the PAZ.

B. Large exhumation event at time t_1 forms exhumed PAZ_1. A new PAZ forms at depth.

C. Section is buried and reheated beneath sediments of a sedimentary basin at time t_2. Heating resets all apatites below their respective T_a. Exhumed PAZ_1 is partially reset. In the lower part of the current PAZ, cooling paths for apatites with different T_a may be parallel. If the exhumation event was large enough to shift the entire PAZ_1 to a temperature hotter than the appropriate T_a, then the exhumed PAZ1 would be completely overprinted.

D. A second large exhumation event creates new exhumed PAZ_2 at time t_3. Ongoing exhumation could subsequently expose the entire exhumed PAZ in mountainous topography. If the simplifying thermal assumptions are correct, the shape of the age-elevation curve can be used to reconstruct the magnitude of thermal events. The difference between the magnitude of exhumation t_1 (a) and burial (b) is equal to the difference between the base of PAZ_1 and the base of PAZ_2 (c) (for a given apatite type). Therefore, if the base of PAZ_1 and PAZ_2 can be determined and the magnitude of burial can be constrained by thermal modeling or independent geological data, it is possible to estimate the magnitude of exhumation that occurred at t_1.

Figure 7. Fission-track age plotted versus elevation for the Boom Gorge, Shamsi, Issyk Ata, and Ala Archa sections (from left to right; east to west). All samples are plotted on a common vertical axis. Boom Gorge is in the footwall; other sections are in the hanging wall. Inset in upper right shows the young portion of the 3 hanging wall sections. Numbers next to samples indicate kinetic character of apatite; italics denote wt%Cl; normal text denotes Dpar. Ala Archa data is from ***Bullen et al.*** [2003]; Dpar values from this profile are not directly comparable with other Dpar values shown as Dpar measurements depend on both the operator and the etching conditions [*Sobel et al.*, 2004]. Upper dashed line indicates the maximum peak elevation. Lower dashed line indicates position of base of exhumed PAZ for low-chlorine apatite. Fine dashed line shows approximate age-elevation path, constructed following Fig. 6. Amount of exhumation calculated using a geothermal gradient of 26°C/km [*Gubin*, 1986] and the T_a (Table 2). Thermal conductivity of young sediments and basement were not differentiated. Grey region indicates average thickness of sedimentary basin that could have formerly overlain the range; the upper and lower limits are ± ca. 300 m. The image at the top shows a Multispectral scanner image draped over an SRTM DEM, depicting the view of the range looking from the north. White circles denote the location of partially reset fission-track samples; grey circles denote fully reset samples.

Figure 8. Representative track-length models for the Shamsi and Boom Gorge profiles. See text for modeling details. Boom Gorge sample modeled using 0.07wt% Cl, chosen by comparison with other samples to be equivalent to Dpar of 1.70 μm.

Figure 9. Schematic evolution of topography in the Kyrgyz range, showing the effect of contrasting lithologies on exhumation and surface uplift rates.

A. Oligocene Early Miocene foreland basin deposited above regional erosion surface.

B. Rapid exhumation of sediments in hanging wall of thrust causes rapid cooling but slow surface uplift of range.

C As the area of exposed basement increases relative to young sedimentary cover, erosion rates decrease, leading to increasing surface uplift rates.

D. Range becomes large enough to create an orographic barrier and subsequently place upper portion of the range above the Equilibrium Line Altitude (ELA). Glacial erosion causes drainage basins on windward side to expand at the expense of more arid, less deeply incised basins on the leeward side.

Figure DR1. Characterization of apatite samples. Compositional data are plotted for all samples. Track-length histograms are only plotted for samples with a significant number of measurements.

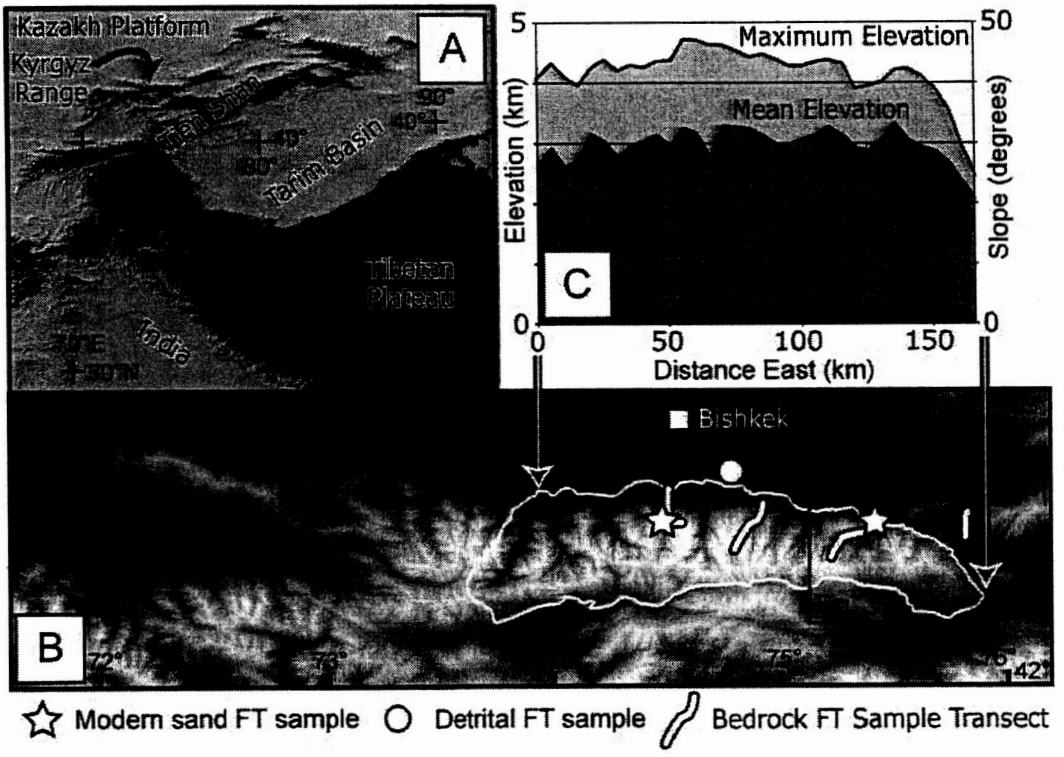

Figure 1, Sobel et al.

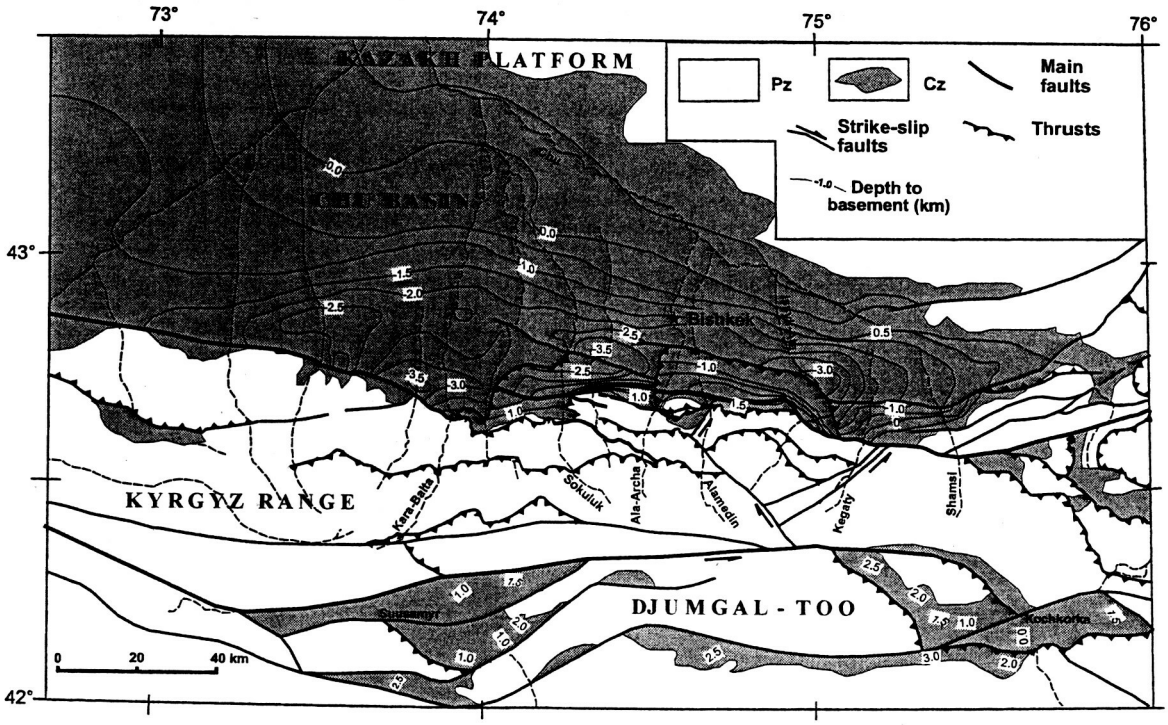

Figure 2, Sobel et al.

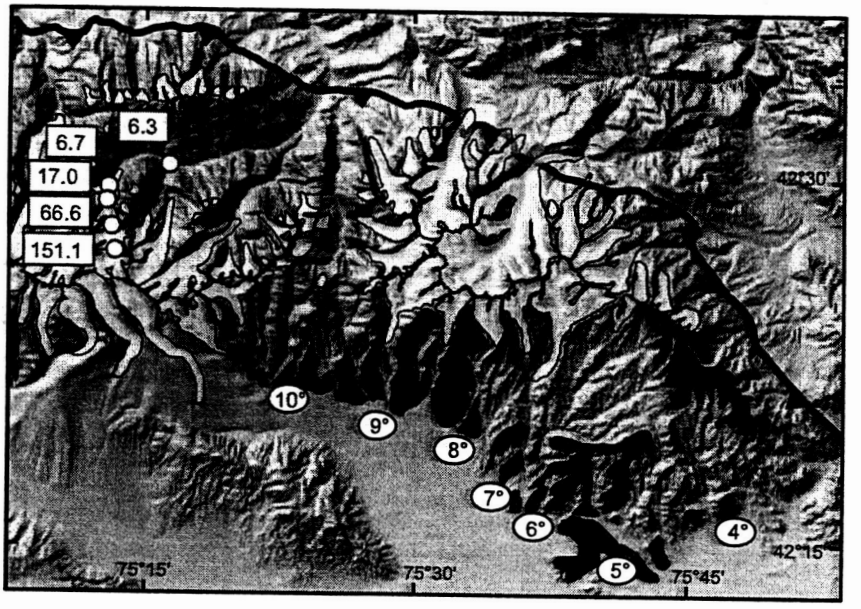

Figure 3, Sobel et al.

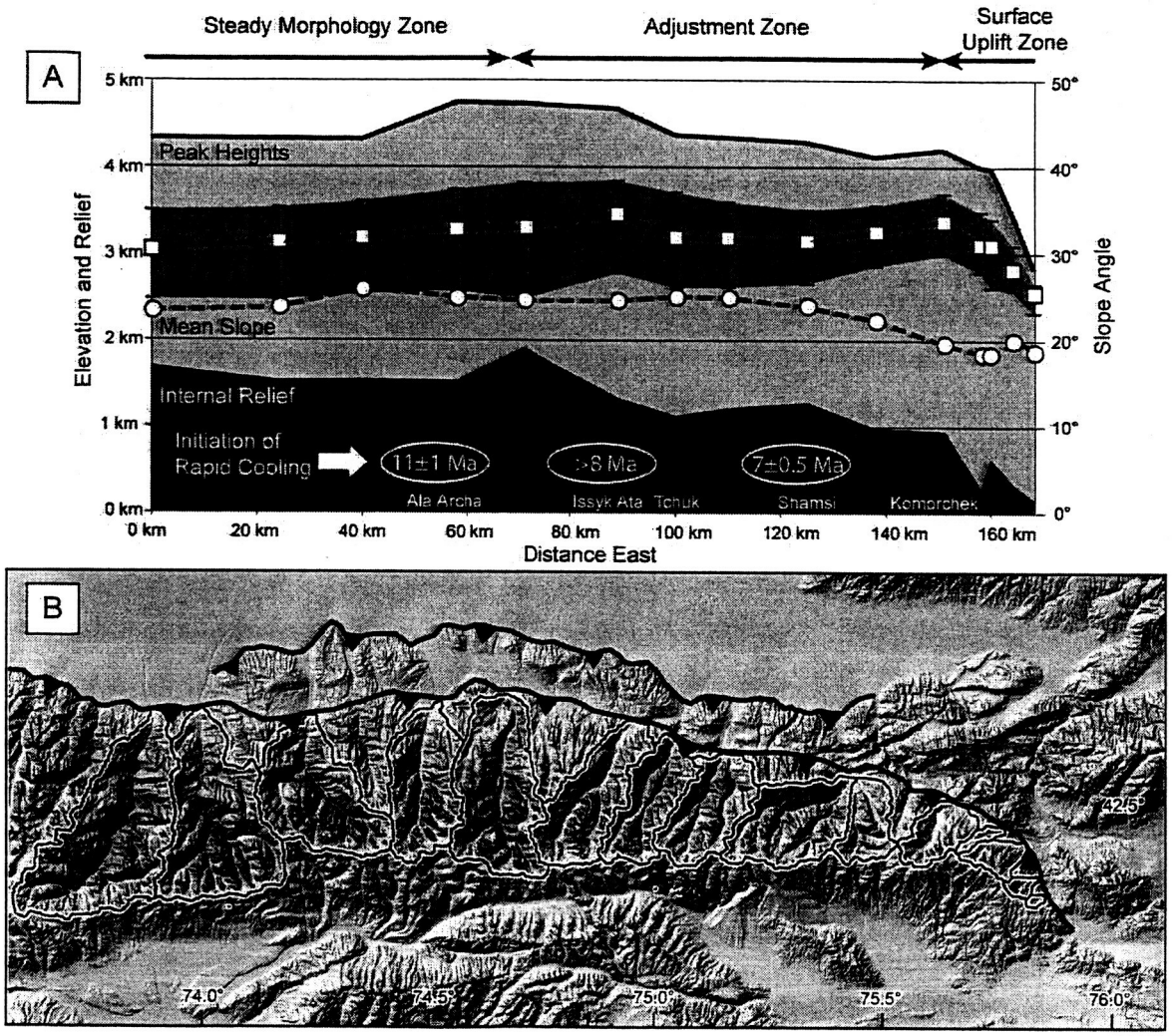

Figure 4, Sobel et al.

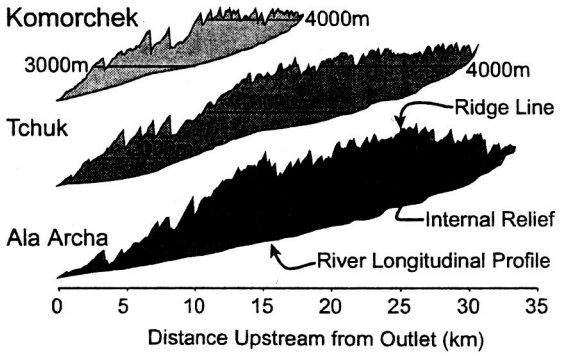

Figure 5, Sobel et al.

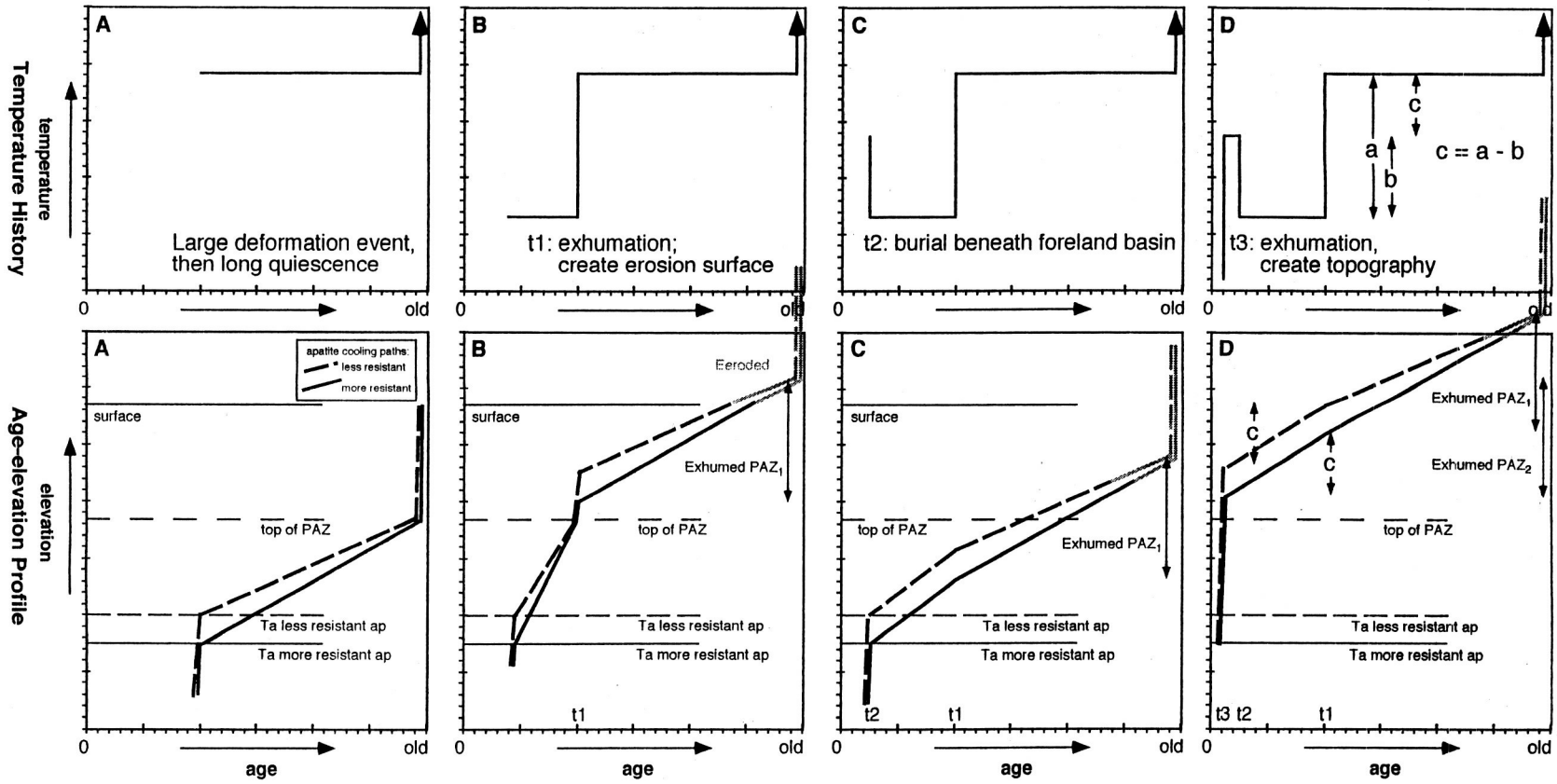

Figure 6. Sobel et al.

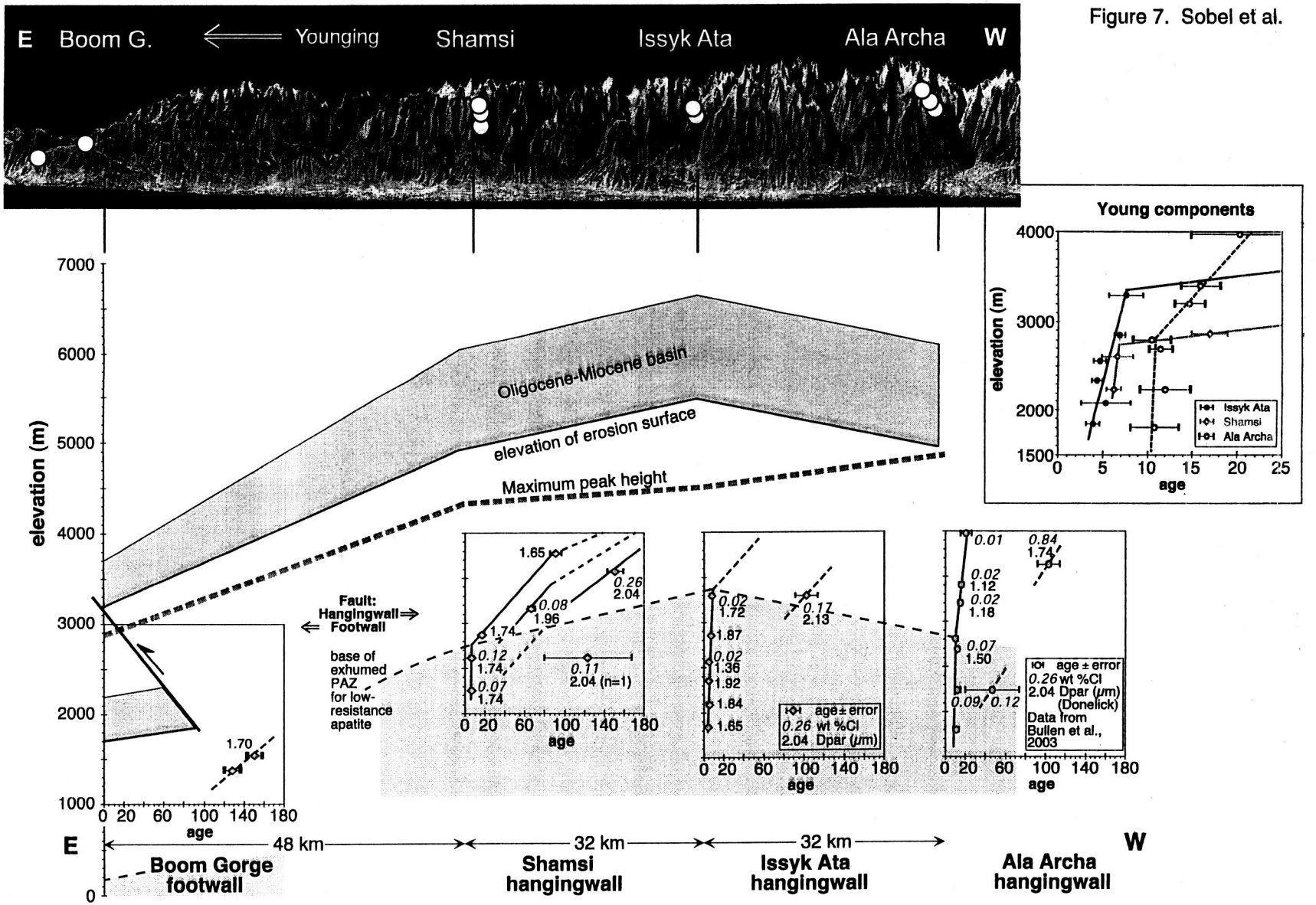

Figure 7. Sobel et al.

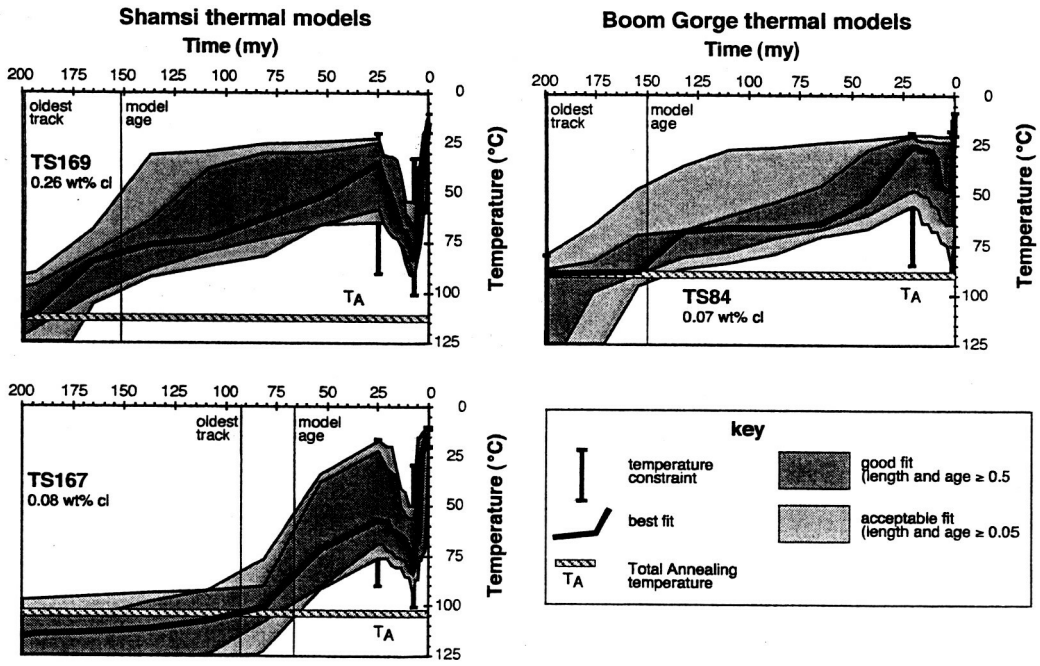

Figure 8, Sobel et al.

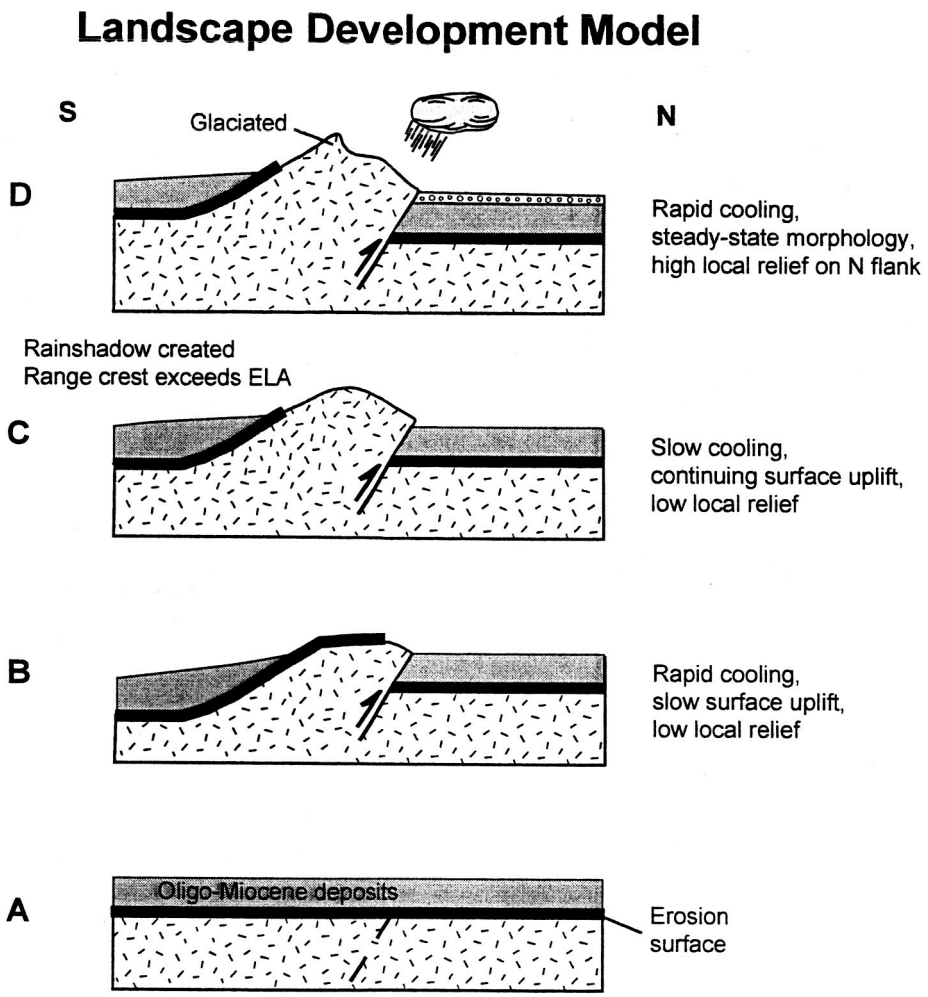

Figure 9, Sobel et al.

Table 1. Fission track data from the Kyrgyz range

sample	irradiation code	comp-onent	age	lithology	N long	E lat	altitude (gps) m	altimeter m	No Xl*	Rho-S ($x10^5$)†	NS §	Rho-I ($x10^5$)†	NI §	P(χ^2) (%)	Rho-D ($x10^6$) **	ND ††	Age (Ma)	±1σ error	U ppm	Dpar (μm)	stdev (μm)	Cl wt%	length (μm)	error (μm)	stdev (μm)	No lengths
Issyk Ata					42°	74 °																				
TS161	UP32-13+		O3	granite	30.108	52.901	3350	3290	31	1.9880	145	11.750	857	0	1.3330	5420	24.5	7.6	11.0	1.85	0.29	0.10	12.92	0.32	1.63	26
	UP43-6+	young							25	0.3097	17	10.040	551	93	1.3330	5420	7.6	1.9	9.4	1.72	0.16	0.02				
	UP43-7	old							6	7.0970	128	16.980	306	0	1.3330	5420	102.0	11.0	15.9	2.13	0.34	0.17				
TS159	UP32-12		O3	granite	31.108	52.425	na	2850	20	1.0280	132	33.790	4338	8	1.2330	5034	6.9	0.6	34.3	1.87	0.14		13.50	0.49	1.37	8
TS158	UP32-11		O3	granite	32.364	52.178	2560	2560	25	0.5357	47	25.620	2248	99	1.2260	5034	4.7	0.7	26.1	1.36	0.09	0.02				0
TS162	UP43-8		O3	granite	33.391	53.351	2380	2350	31	0.4456	59	24.740	3275	24	1.3240	5420	4.4	0.6	23.4	1.92	0.08		13.44	0.07	0.10	2
TS163	UP43-9		R	metavolc	34.854	54.187	2060	2090	4	0.4827	4	21.600	179	74	1.3140	5420	5.4	2.8	20.5	1.84	0.35					0
Mav38	UP65-10+11		O3	granite	37.912	55.100	1840		34	0.2850	34	1.480	1765	93	1.0847	4531	3.9	0.7	17	1.65	0.25					
Shamsi					42°	75 °																				
TS170	UP32-16		C2-3	sandstone	27.344	14.024	3865	3770	22	4.814	636	12.120	1601	4	1.2580	5034	91.1	5.6	12.0	1.65	0.13	0.12	12.58	0.33	1.53	22
TS169	UP32-15		C1	sandstone	27.751	13.944	3697	3570	19	16.2100	836	24.530	1265	22	1.2520	5034	151.1	7.7	24.5	2.04	0.16	0.26	12.06	0.17	1.69	100
TS167	UP43-12		C1	sandstone	28.237	13.135	3254	3160	24	4.0790	661	14.470	2344	18	1.2850	5420	66.6	3.4	14.1	1.96	0.14	0.10	11.89	0.26	1.88	52
TS166	UP32-14		C1	sandstone	29.301	12.973	2930	2870	22	1.0780	146	13.930	1886	35	1.2450	5034	17.0	2.0	14.0	1.74	0.15		14.38	0.47	0.95	4
TS165	UP43-11		C1	sandstone	29.830	12.996	2670	2610	12	0.6100	27	12.700	562	0	1.2950	5420	13.7	7.0	12.3	1.80	0.21	0.12	12.95			1
		young							11	0.3629	15	13.040	539	62	1.2950	5420	6.7	1.8	12.6	1.74	0.17	0.12				
		old							1	4.1030	12	7.864	23	na	1.2950	5420	123.6	44.1	7.6	2.04	na	0.11				
TS164	UP43-10		C1	sandstone	30.739	16.158	2280	2250	20	0.3551	63	13.590	2412	85	1.3040	5420	6.3	0.8	13.0	1.74	0.11	0.07	11.99	0.97	2.57	7
Boom Gorge					42°	75 °																				
TS84	UP30-17		P	granite	32.688	48.867	1530	1620	20	9.694	826	15.410	1313	84	1.3070	5224	150.2	7.6	14.7	1.70	0.11		12.50	0.23	1.99	73
TS27	UP2-20		D-C3	sandstone	38.010	50.562	1376	na	12	6.378	569	9.394	838	12	1.0510	4299	127.5	10.1	11.2	na	na		12.82	0.20	1.96	100

Notes: Sample preparation and analysis were similar to that outlined in Sobel and Strecker (2003). Samples analyzed with a Leica DMRM microscope with drawing tube located above a digitizing tablet and a Kinetek computer-controlled stage driven by the FTStage program (Dumitru, 1993). Analysis performed with reflected and transmitted light at 1250x magnification. Samples were irradiated at Oregon State University, USA except TS27, which was irradiated at Risø National Laboratory, Denmark . Following irradiation, the mica external detectors were etched with 21°C, 40% hydrofluoric acid for 45 minutes. The pooled age (central age) is reported for samples with P(χ^2) greater than (less than) 5% as they pass (fail) the χ^2 test; error is one sigma, calculated using the zeta calibration method (Hurford and Green, 1983) with zeta of 369.6 ± 7.6 for apatite (E. Sobel, unpublished). Sample TS27 calculated with a zeta of 361±20 (E. Sobel, unpublished). Note that 3 slides were combind for sample TS161 and 2 for Mav38.

*No Xls is the number of individual crystals dated. †Rho-S and Rho-I are the spontaneous and induced track density measured, respectively (tracks/cm^2). §NS and NI are the number of spontaneous and induced tracks counted, respectively. #P(χ^2) (%) is the chi-square probability (Galbraith, 1981; Green, 1981). **Rho-D is the induced track density in external detector adjacent to CN5 dosimetry glass (tracks/cm^2). ††ND is the number of tracks counted in determining Rho-D. Microprobe measurements were performed with PAP correction procedures, operating conditions of 15kV beam, beam current of 20 nA (measured on a Faraday cup) and a ca. 15 μm beam diameter. Chlorine was measured for 100 seconds, providing a ca. 150 ppm detection limit. Calibration included a Durango apatite standard which was repeatedly measured during the course of analysis.

Table 2. Summary of AFTSolve model results.

	TS169		TS167	
	min	max	min	max
Ta (°C)	112	113	100	103
Tmin (°C), pre-Cz seds	35	50	57	57
Tmax (°C) beneath Cz seds	81	84	75	82
burial beneath Cz seds (km)	1.2	1.8	0.7	1.0
Wt% Cl		0.26		0.08

Data summarized from all model runs that yielded good fits to the observed data.